Referee #1

We thank the reviewer for a thoughtful and thorough review of our manuscript (ESSD-2023-87: SinoLC-1: the first 1-meter resolution national-scale land-cover map of China created with the deep learning framework and open-access data). The suggestions and comments are listed in **bold** type. The modified words or materials are marked as blue color in the revised manuscript. The item-by-item responses to all comments are listed below.

General comments:

The SinoLC-1 product, the initial 1-m resolution land cover data product for China, is introduced in this work. It may be useful for understanding fine-scale biogeophysical issues on the land. Also, the product offers development in big data processing, sample migration, and open-access data application that might be useful for efficient national land resource surveys and the mapping of large-scale very-high-resolution land cover data. Before it may be accepted, this manuscript should yet be improved.

Response:

We are particularly grateful for your careful reading, and for giving us many constructive comments on this work. According to the suggestions and comments, we have carefully considered all of them and tried our best to improve the manuscript.

Suggestions and comments:

(1) The Introduction, which focuses on data at the global scale, highlights 3 types of land use land cover data that fully or partially cover China. Reviewing national and local-scale land use land cover data in China is advised given that this manuscript focuses on the production of land cover maps at the national scale. The CLCD and CLUD in China and the NLCD in the United States are examples of the several extensively utilized national-scale land use land cover product.

Response:

We appreciate this suggestion from the reviewer and agree that reviewing the various achievements of researchers in national-scale land-cover products enables us to improve the logicality of the introduction part and make the manuscript more complete.

Based on the suggestions, we supplemented the types of 'National-scale moderate-/high-resolution land-cover products' in the Introduction Section and carefully collected the materials of five high-quality national-scale land-cover products. Furthermore, to clearly demonstrate various types of land-cover datasets reviewed in the manuscript, we summarized their information and reference sources in Table R1-1.

The supplement materials include:

- The 30-m resolution National Land Cover Database (NLCD) covering the whole United States, which is cyclically updated by the United States Geological Survey (USGS) with the Landsat imagery (Wickham et al., 2021);

- The 10-m resolution LCM2020 covering the whole United Kingdom, which is periodically published by the United Kingdom Centre for Ecology & Hydrology (UKCEH) with the Sentinel imagery (Morton et al., 2021);

- The 30-m China Land Use Dataset (CLUD) covering the whole China from the 1980s to 2015 at an interval of 5 years, which was produced by the Chinese Academy of Sciences with multitemporal Landsat imagery (Liu et al., 2014);

- The 30-m China Land Cover Dataset (CLCD) covering the whole China from 1990 to 2019 annually, which was produced by Wuhan University with multitemporal Landsat imagery and Google Earth Engine (Yang & Huang 2021).

- The 10-m Cross Resolution Land Cover (CRLR 2020) covering the whole China in the year 2020, which was generated by Wuhan University with Sentinel imagery and deep learning framework (Liu et al., 2023).

Table R1-1. Different types of land-cover datasets reviewed in the manuscripts. The supplements are colored in blue.

Type	Spatial resolution	Image source	Affiliation	Published year	Coverage	Reference
Global LR land-cover product	1000m	SPOT4	EC-JRC	2007	Global	Bartholomé, E., & Belward, A. S. (2007). GLC2000 : a new approach to global land cover mapping from Earth observation data. 1161. https://doi.org/10.1080/01431160412331291297
	1000m	AVHRR	EC-JRC and USGS	2010	Global	Loveland, T. R., Reed, B. C., Brown, J. F., Ohlen, D. O., Zhu, Z., & Yang, L. (2010). Development of a global land cover characteristics database and IGBP DISCover from 1 km AVHRR data. 1161. https://doi.org/10.1080/014311600210191
	500m	MODIS	USGS and NASA	2009	Global	Friedl, M. A., Sulla-menashe, D., Tan, B., Schneider, A., Ramankutty, N., Sibley, A., & Huang, X. (2010). Remote Sensing of Environment MODIS Collection 5 global land cover : Algorithm re fi nements and characterization of new datasets. Remote Sensing of Environment, 114(1), 168–182. https://doi.org/10.1016/j.rse.2009.08.016
Global MR/HR land-cover product	30m	Landsat	Tsinghua University	2013	Global	Gong, P., Wang, J., Yu, L., Zhao, Y., Zhao, Y., Liang, L., Yu, L., Wang, L., Liu, X., Shi, T., Zhu, M., Chen, Y., Yang, G., Tang, P., Xu, B., Giri, C., Clinton, N., Zhu, Z., Chen, J., & Chen, J. (2013). Finer resolution observation and monitoring of global land cover : first mapping results with Landsat TM and ETM + data. 1161. https://doi.org/10.1080/01431161.2012.748992
	30m	Landsat and Huanjing-1	National Geomatics Center of China	2015	Global	Chen, J., Chen, J., Liao, A., Cao, X., Chen, L., Chen, X., He, C., Han, G., Peng, S., Lu, M., Zhang, W., Tong, X., & Mills, J. (2015). ISPRS Journal of Photogrammetry and Remote Sensing Global land cover mapping at 30 m resolution: A POK-based operational approach. ISPRS Journal of Photogrammetry and Remote Sensing, 103, 7 –27. https://doi.org/10.1016/j.isprsjprs.2014.09.002
	30m	Lansat	Chinese Academy of Sciences	2021	Global	Zhang, X, Liu, L., Chen, X., Gao, Y., Xie, S., & Mi, J. (2021). GLC_FCS30: global land-cover product with fine classification system at 30 m using time-series Landsat imagery. *Earth Syst. Sci. Data* , *13*(6), 2753–2776. https://doi.org/10.5194/essd-13-2753-202
	10m	Sentinel	Tsinghua University	2019	Global	Gong, P., Liu, H., Zhang, M., Li, C., Wang, J., Huang, H., Clinton, N., Ji, L., Li, W., Bai, Y., Chen, B., Xu, B., Zhu, Z., & Yuan, C. (2019). Stable classification with limited sample : transferring a 30-m resolution sample set collected in 2015 to mapping 10-m resolution global land cover in 2017. 64, 370 – 373. https://doi.org/10.1016/j.scib.2019.03.002
	10m	Sentinel	ESA	2021	Global	Van De Kerchove, R., Zanaga, D., Keersmaecker, W., Souverijns, N., Wevers, J., Brockmann, C., Grosu, A., Paccini, A., Cartus, O., & Santoro, M. (2021). ESA WorldCover: Global land cover mapping at 10 m resolution for 2020 based on Sentinel-1 and 2 data. AGU Fall Meeting Abstracts, 2021, GC45I-0915.
	10m	Sentinel	ESRI Inc. and IO Inc.	2021	Global	Karra, K., Kontgis, C., Statman-weil, Z., Mazzariello, J. C., Mathis, M., Steven, P., & Observatory, I. (n.d.). Global land use / land cover with Sentinel 2 and deep learning.
National MR/HR land-cover product	30m	Lansat	USGS	Since 2001	National (USA)	Wickham, J., Stehman, S. V, Sorenson, D. G., Gass, L., & Dewitz, J. A. (2021). Thematic accuracy assessment of the NLCD 2016 land cover for the conterminous United States. Remote Sensing of Environment, 257, 112357
	10m	Sentinel	UKCEH	Since 2015	National (UK)	Morton, R. D., Marston, C. G., O' Neil, A. W., & Rowland, C. S. (2021). Land Cover Map 2020 (10m classified pixels, GB). *NERC EDS Environmental Information Data Centre* . https://doi.org/10.5285/35c7d0e5-1121-4381-9940-75f7673c98f7
	30m	Lansat	Chinese Academy of Sciences	2014	National (CN)	Liu, J., Kuang, W., Zhang, Z., Xu, X., Qin, Y., Ning, J., Zhou, W., Zhang, S., Li, R., & Yan, C. (2014). Spatiotemporal characteristics, patterns, and causes of land-use changes in China since the late 1980s. Journal of Geographical Sciences, 24, 195–210.
	30m	Lansat	Wuhan University	2021	National (CN)	Yang, J., & Huang, X. (2021). The 30m annual land cover dataset and its dynamics in China from 1990 to 2019. Earth System Science Data, 13(8), 3907 – 3925. https://doi.org/10.5194/essd-13-3907-2021
	10m	Sentinel	Wuhan University	2023	National (CN)	Liu, Y., Zhong, Y., Ma, A., Zhao, J., & Zhang, L. (2023). Cross-resolution national-scale land-cover mapping based on noisy label learning: A case study of China. International Journal of Applied Earth Observation and Geoinformation, 118, 103265.
Regional VHR land-cover product	0.3m	Google Earth and airborne images	Wuhan University	2021	3 cities of CN	Wang, J., Zheng, Z., Lu, X., & Zhong, Y. (2021). LoveDA: A Remote Sensing Land-Cover Dataset for Domain Adaptive Semantic Segmentation. Thirty-Fifth Conference on Neural Information Processing Systems Datasets and Benchmarks Track (Round 2).
	2.1m	Ziyuan-3	Wuhan University	2020	42 cities of CN	Huang, X., Wang, Y., Li, J., Chang, X., Cao, Y., Xie, J., & Gong, J. (2020). High-resolution urban land-cover mapping and landscape analysis of the 42 major cities in China using ZY-3 satellite images. Science Bulletin, 65(12), 1039 – 1048. https://doi.org/10.1016/j.scib.2020.03.003
	2.4m	Google Earth, Ziyuan-3,and Gaofen-6	Peking University	2020	81 cities of CN	Du, S., Du, S., Liu, B., Zhang, X., & Zheng, Z. (2020). Large-scale urban functional zone mapping by integrating remote sensing images and open social data. GIScience & Remote Sensing, 57(3), 411–430. https://doi.org/10.1080/15481603.2020.1724707

The cited references of the national-scale moderate-/high-resolution land-cover datasets are as follows:

Wickham, J., Stehman, S. V, Sorenson, D. G., Gass, L., & Dewitz, J. A. (2021). Thematic accuracy assessment of the NLCD 2016 land cover for the conterminous United States. Remote Sensing of Environment, 257, 112357. https://doi.org/10.1016/j.rse.2021.112357

Morton, R. D., Marston, C. G., O' Neil, A. W., & Rowland, C. S. (2021). Land Cover Map 2020 (10m classified pixels, GB). NERC EDS Environmental Information Data Centre. https://doi.org/10.5285/35c7d0e5-1121-4381-9940-75f7673c98f7

Liu, J., Kuang, W., Zhang, Z., Xu, X., Qin, Y., Ning, J., Zhou, W., Zhang, S., Li, R., & Yan, C. (2014). Spatiotemporal characteristics, patterns, and causes of land-use changes in China since the late 1980s. Journal of Geographical Sciences, 24, 195–210. https://doi.org/10.1007/s11442-014-1082-6

Yang, J., & Huang, X. (2021). The 30m annual land cover dataset and its dynamics in China from 1990 to 2019. Earth System Science Data, 13(8), 3907–3925. https://doi.org/10.5194/essd-13-3907-2021

Liu, Y., Zhong, Y., Ma, A., Zhao, J., & Zhang, L. (2023). Cross-resolution national-scale land-cover mapping based on noisy label learning: A case study of China. International Journal of Applied Earth Observation and Geoinformation, 118, 103265. https://doi.org/10.1016/j.jag.2023.103265

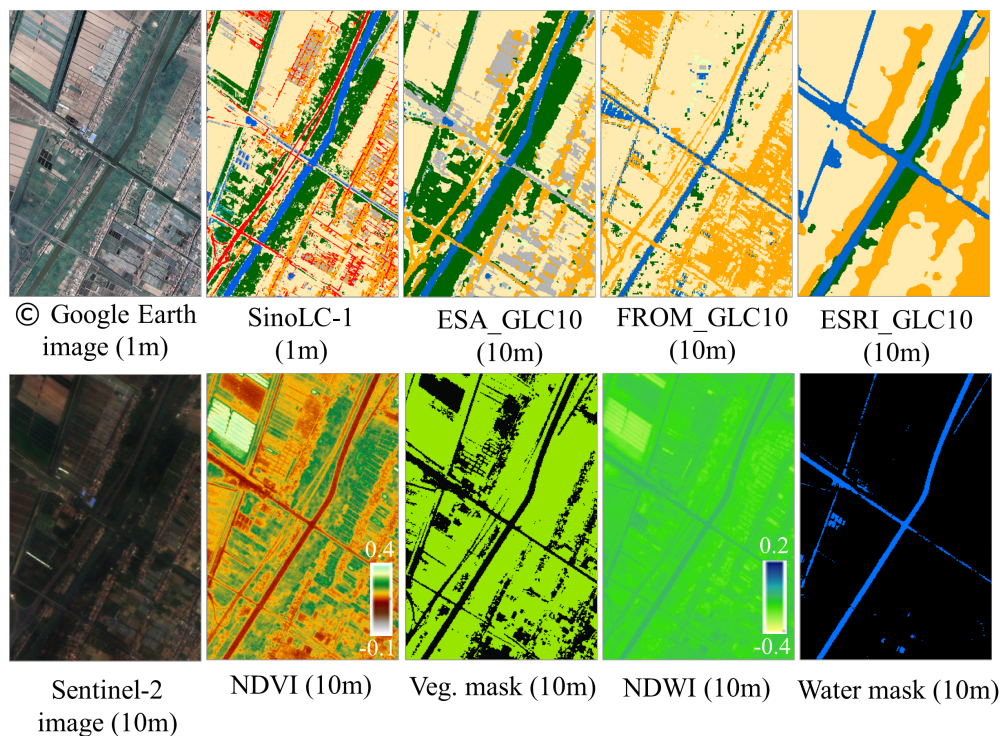**(2) Why not use bands composition to assist in mapping?**

Response:

Thank you for the constructive comment. We have carefully considered this question during the production process of SinoLC-1. Since the VHR Google Earth images contain three basic bands which are difficult to apply common band composition process, we agree that using multi-spectral images (e.g., Sentinel-2) or composition index data (e.g., NDVI, NDWI, etc.) enables to assist the mapping process. Specifically, I would like to respond this comment from three aspects, which are concluded during the practical production of the SinoLC-1:

- (1/3) The additional information provided by multi-spectral images and band composition data.

    In the moderate-/high-resolution land-cover mapping process, multi-spectral images from Landsat or Sentinel mission general provide abundant spectral information which can better distinguish confused land-cover types. This enables land-cover products produced based on these images to contain reasonable classification results on these confused land-cover types. The production process of SinoLC-1 was based on the classification results of these multi-spectral

images, where these products (i.e., ESA_GLC10, FROM_GLC10, and ESRI_GLC10) were used as training labels. By combining the rich labeled information of these training labels and the fine edge and texture information of three band VHR Google images, the classification results based on multi-spectral images with a fine edge and details can be learned and inherited by SinoLC-1 to a certain extent.

As shown in the top row of Figure R1-1, SinoLC-1 has learned and inherited these classification results (e.g., water, vegetation, impervious) of 10-m GLC produced by using multispectral images. As shown in the bottom row of Figure R1-1, we collected the multi-spectral Sentinel-2 image from the same location and used common band composition to generate index data for NDVI and NDWI, the information contained in the index data is basically reflected in the GLC training labels.

| © Google Earth image (1m) | SinoLC-1 (1m) | ESA_GLC10 (10m) | FROM_GLC10 (10m) | ESRI_GLC10 (10m) |

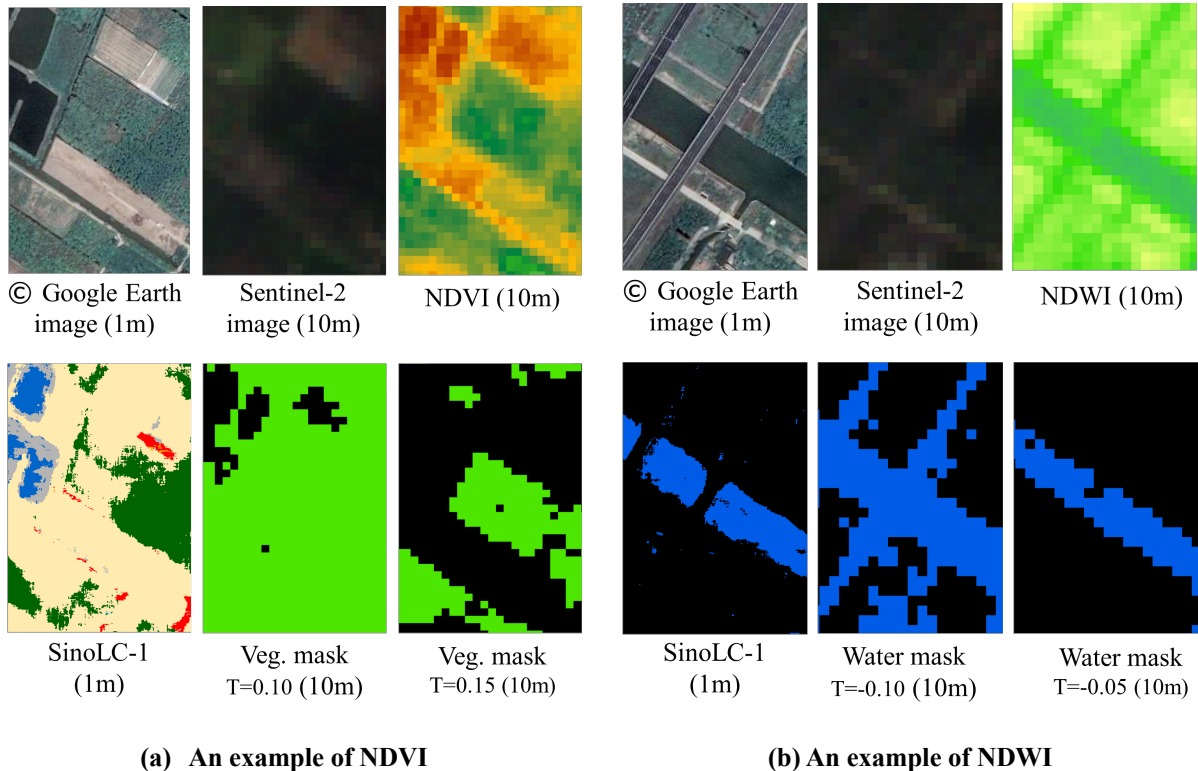| Sentinel-2 image (10m) | NDVI (10m) | Veg. mask (10m) | NDWI (10m) | Water mask (10m) |

Figure R1-1. Demonstration of different data in a sample area of Shanghai.

- (2/3) The mismatched resolution between the VHR optical images, multi-spectral images, and band composition index data.

    The 10-m Sentinel-2 imagery, as a suitable multi-spectral auxiliary data to conduct band composition, has a 10 times spatial resolution discrepancy to the using VHR Google Earth images. As shown in the top row of Figure R1-2, the mismatched resolution between the VHR

optical images, multi-spectral images, and band composition index data can cause data offset when they are input to the network for training. Furthermore, the land-cover mapping network used in this manuscript includes a resolution-preserving backbone, a weakly supervised label selection module, and a self-supervised loss function. Although the network performs well in resolving the resolution offset between images and labels by highly preserving the resolution of extracted features, the land-object edge and spatial detail of the mapping results inevitably rely on the input VHR images. Besides, in our previous works, we have validated that taking multi-spectral images with lower resolution as auxiliary data for the VHR land-cover mapping process can bring in abundant spectral information, but reduce the spatial details of the mapping results.

Figure R1-2 shows the masks generated from the index data by setting different thresholds. In addition to the resolution offset between these data, different threshold setting has a significant impact on the mask generated by these band composition index data. In the national-scale land-cover mapping process, the variation of band composition index data in different regions can make it difficult to select appropriate thresholds for mask generation.

| © Google Earth image (1m) | Sentinel-2 image (10m) | NDVI (10m) | © Google Earth image (1m) | Sentinel-2 image (10m) | NDWI (10m) |

| SinoLC-1 (1m) | Veg. mask T=0.10 (10m) | Veg. mask T=0.15 (10m) | SinoLC-1 (1m) | Water mask T=-0.10 (10m) | Water mask T=-0.05 (10m) |

(a) An example of NDVI   (b) An example of NDWI

Figure R1-2. Demonstration of the index data generated by the band composition

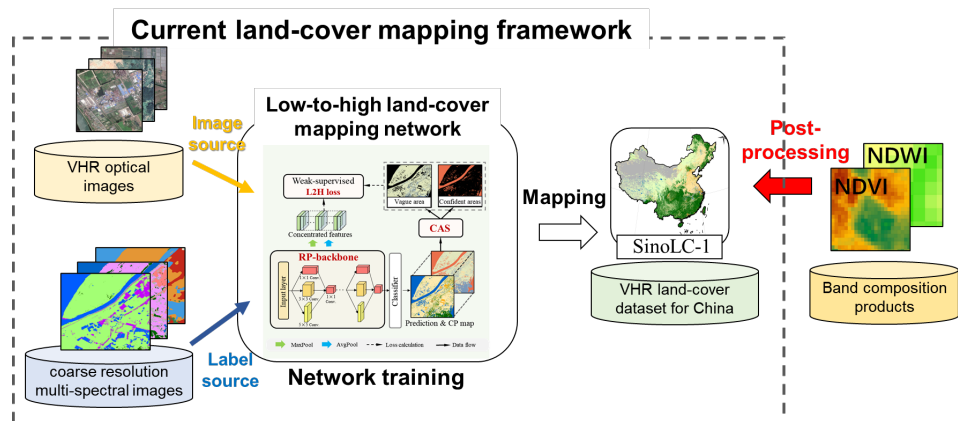- (3/3) Discussion on two ways of using band composition to assist the VHR national-scale land-cover mapping.

Based on the above-mentioned analysis, we have listed two suitable ways to use band composition to assist VHR national scale land cover mapping after fully considering the utilized framework and calculation resources. As shown in Figure R1-3, the listed two ways include: (a) Using Sentinel-2 imagery as auxiliary data to the VHR optical imagery and (b) Using band composition index data as post-processing data to the SinoLC-1 dataset.

(a) By combining the 13 multi-spectral bands of Sentinel-2 images with the current VHR images to reconstruct the input image data is a basic method to assist the land-cover mapping process. As shown in Figure R1-3 (a), this combination can maximize the utilization of spectral information provided by the Sentinel-2 image. However, in addition to the abovementioned resolution offset issue between different image sources, it requires us to collect the Sentinel-2 images covering the whole China, and the reconstructed image contains a large number of channels, which relies on more computational and storage capabilities for conducting the national-scale mapping process.

(b) By calculating the band composition index data and using them to assist the post-processing of the mapping results is another suitable method to improve the quality of the SinoLC-1 dataset. As shown in Figure R1-3 (b), with the index data (e.g., NDVI, NDWI, etc.) calculated based on multispectral images, it is possible to correct the misclassification land-cover types and improve the overall quality of the SinoLC-1. The advantage of such a method is that it does not require the reconstruction of training data (especially the images) and model retraining, but only uses appropriate band composition data to post-process the results. Therefore, we are trying our best to utilize the index data generated by the Sentinel-2 image to improve the current results and reevaluate the accuracy. In future work, we continue to reevaluate the improved results and update the dataset.
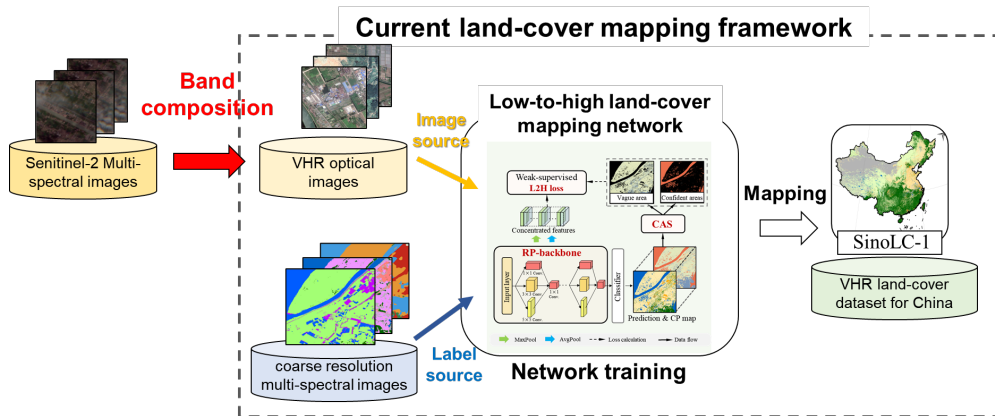
(a) Using Sentinel-2 imagery as auxiliary data to the VHR optical imagery

(b) Using band composition index data as post-processing data to the SinoLC-1 dataset.

Figure R1-3. Two ways of using band composition to assist the VHR national-scale land-cover mapping.

(3) Why are other OSM types not involved in mapping?

Response:

Thanks for the question. Before conducting the national-scale land-cover mapping, we conducted thorough research on the selection of input data. Open Street Map (OSM), as one of the most popular volunteer geographic information data sources, allows everyone in the community to edit the maps. As shown in Figure R1-4, OSM contains three types of data: points of interest, traffic routes, and polygons. Among them, the points of interest are usually labeled coordinate points without a systematic classification system. For example, in the example of Shanghai, the points of interest are labeled with the names of different restaurants, hotels, and coffee shops, which makes them difficult to utilize in land-cover mapping tasks. For polygons, their corner points are manually
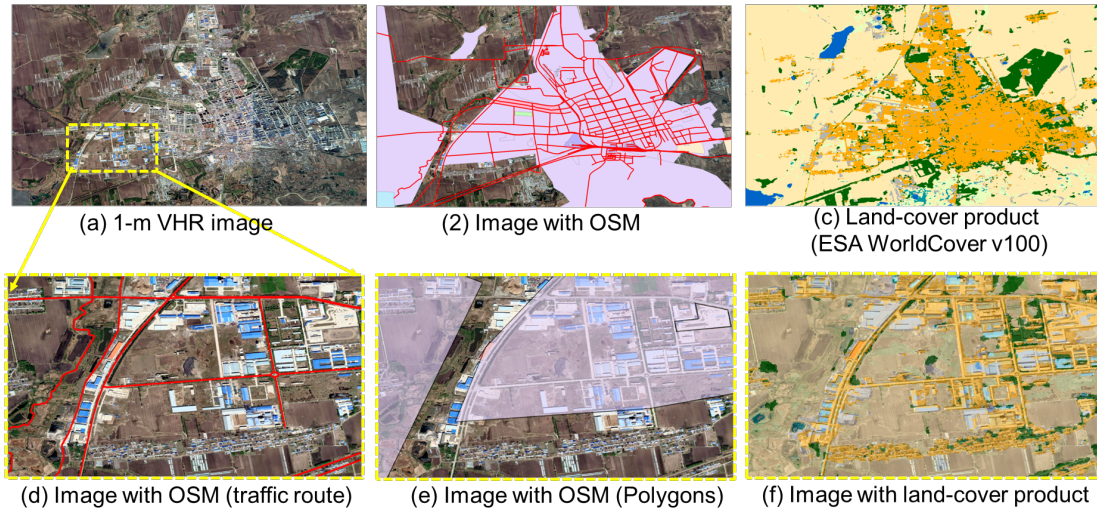
labeled, and their attributes contain the basic land use types (such as commercial, industrial, etc.). For traffic routes, they are usually labeled by uploaders who carried with GPS receivers and updated to OSM by walking, cycling, or driving along the road. Based on this, traffic routes usually have more accurate labeling information.
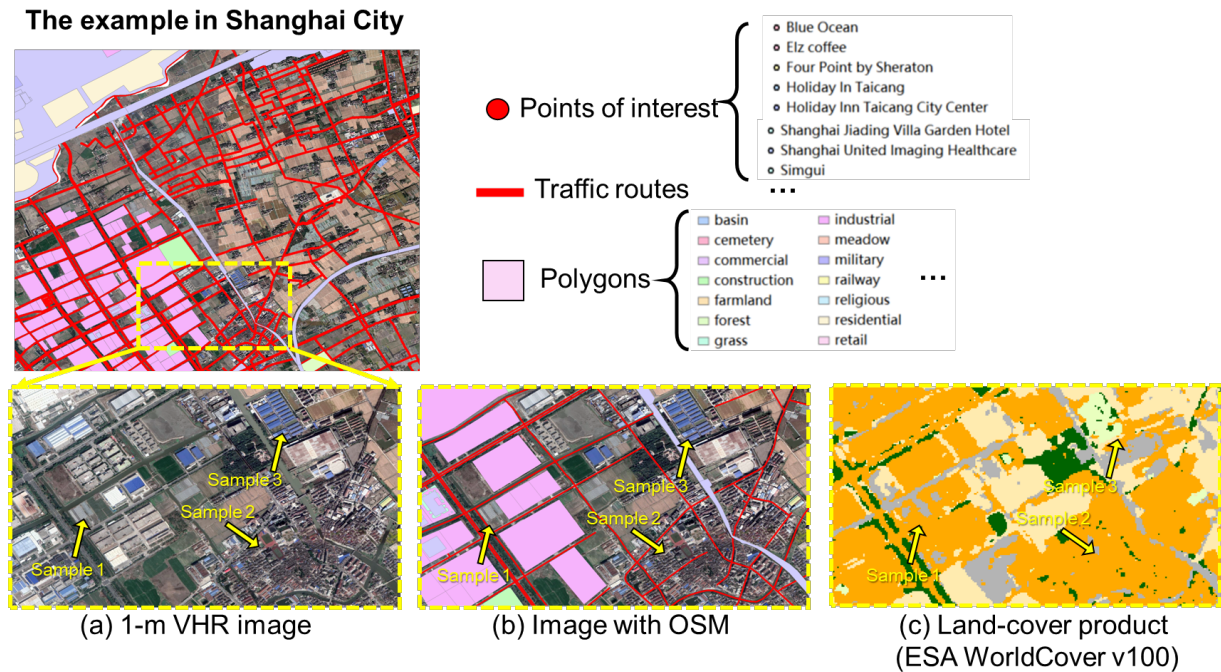
Figure R1-4. Demonstration of the OSM data in Shanghai City.

To demonstrate different types of data in the OSM, we selected three sample areas in Figure R1-4 (a). For sample 1, it can be found that OSM's polygons data does not accurately label the boundaries of 'industrial', but instead labels most of the area of a factory. For samples 2 and 3, it can be observed that due to the inaccurate manual-annotation of OSM's polygons data, many basic land-use types such as industrial and residential areas in the same area miss annotation information. Figure R1-4 (c) shows the land-cover product which was used in the training process of the SinoLC-1. Since the land-cover products are interpreted from the remote-sensing images rather than manually annotating, the information provided by land-cover products is more complete.

The example in Heihe City

(a) 1-m VHR image

(2) Image with OSM

(c) Land-cover product
(ESA WorldCover v100)

(d) Image with OSM (traffic route)

(e) Image with OSM (Polygons)

(f) Image with land-cover product

Figure R1-5. Demonstration of the OSM data in Heihe City, Heilongjiang Province.

Furthermore, Figure R1-5 shows another example of OSM data in Heihe City, Heilongjiang Province. Compared to Shanghai City, Heihe City is sparsely populated and has a lower level of urban development. From Figure R1-5 (d-f), the traffic route data of OSM is accurate, but the polygons data is relatively inaccurate (only labeling a rough area). The land-cover or land-use information provided by the polygons data is far less accurate than the land-cover product.

In general, OSM's traffic route data can provide additional information for land cover mapping tasks. In numerous land-cover mapping studies, OSM's traffic route data is also widely used (Audebert et al 2017; Guzder-Williams et al, 2022; Zhu et al, 2022), because they provide accurate road-labeled information and reflect urban patterns. For the national-scale land-cover mapping process, the examples shown in Figure R1-5 reveal that the data quality of OSM's polygons has significant differences in different regions, and inaccurate manual-annotation may also bring more label noise. Therefore, in the production of SinoLC-1, we obtained the land-cover information from three GLC products, and only extracted the accurate traffic route data from the OSM to construct the training labels.

The cited references of this response are as follows:

Guzder-Williams, B., Mackres, E., Angel, S., Blei, A.M. and Lamson-Hall, P., 2023. Intra-urban land use maps for a global sample of cities from Sentinel-2 satellite imagery and computer vision. Computers, Environment and Urban Systems, 100, p.101917. https://doi.org/10.1016/j.compenvurbsys.2022.101917

Zhu, Q., Lei, Y., Sun, X., Guan, Q., Zhong, Y., Zhang, L. and Li, D. (2022). Knowledge-guided land pattern depiction for urban land use mapping: A case study of Chinese cities. Remote Sensing of Environment, 272, p.112916. https://doi.org/10.1016/j.rse.2022.112916

Audebert, N., Le Saux, B. and Lefèvre, S. (2017). Joint learning from earth observation and OpenStreetMap data to get faster better semantic maps. In Proceedings of the IEEE Conference on Computer Vision and Pattern Recognition Workshops 67-75.

(4) It's possible to argue against the classification system's building category. Table 2 compares building to mining land in the NLRS, which is inappropriate because mining land refers to a mine site (see the NLRS land category determination rules published in 2019).

Moreover, optical images and even RGB images should have difficulty classifying forest swamps. The authors are suggested to submit mapping results for land cover types that are challenging to distinguish in medium resolution imagery in order to show the scientific significance and applicability of SinoLC-1.

Response:

Thank you for the constructive comments. For the first comment, we carefully checked the document 'Detailed Rules for the Recognition of Land Classification in the Third National Land Survey (2019)' at the website of the Ministry of Natural Resources of the People's Republic of China (https://m.mnr.gov.cn/zt/td/dscqggtdc/zl/201906/P020190604539900543194.pdf). Indeed, the mining land is inappropriate to be sorted into 'building' type. According to the rules, the type of mining land in NLRS refers to ground production lands such as mining, quarrying, sand (sand) quarries, brick and tile kilns, as well as soil (stone) and tailings storage areas. Therefore, we revised the corresponding land-cover type relationship between the SinoLC-1 products and the 3rd NLRS shown in Table 2 of the manuscript (Table R1-2 of the response letter) and the statistical validation set collected from the third national land resource survey projects shown in Table 3 of the manuscript (Table R1-3 of the response letter). Furthermore, based on the revised classification system and relationship table of the land-cover types, we updated the statistical-level validation results shown in Figures 21−23 of the revised manuscript.

Table R1-2. Corresponding land-cover type relationship between the SinoLC-1 products and the 3rd national land survey.

| SinoLC-1 category	3rd NLRS land-cover type	SinoLC-1 category	3rd NLRS land-cover type
Tree cover	Arbor woodland	Building	Urban land
	Bamboo groves		Administrative towns
	Other woodland		Village land
Shrubland	Shrubland		Airport land
Grassland	Natural grassland		Wharf land
Barren and sparse vegetation	Artificial grassland		Pipeline transportation
	Other grassland		Scenic Spot
	Mining land	Wetland	Forest swamp
Cropland	Paddy field		Shrub swamp
	Irrigated land		Swampy grassland
	Dry cropland		Coastal tidal flat
	Orchard		Inland tidal flat
	Tea plantation		Marshland
	Rubber plantation	Water	River
	Other plantations		Lake
Traffic route	Railway		Reservoir
	Rail transit		Pond
	Highway		Ditch
	Rural road		Hydraulic construction
Snow and ice	Glaciers and snow	Moss and lichen	Tundra

Table R1-3. Statistical validation set collecting from the third national land resource survey projects.

Geo. region	Province/ City	Statistical results of different land-cover types (km²)									
		TR	TC	SL	GL+BL&SV	CL	BD	S&I	WT	WL	M&L
South	Hainan	524	10799	943	173	17047	2468	0	1831	1157	57
	Guangxi	3272	124831	36122	2767	49779	9857	0	7490	1178	94
	Guangdong	3000	106522	1404	2390	32267	17757	0	13423	1683	106
East	Fujian	2000	87427	686	753	18503	7109	0	3731	1874	12
	Anhui	2824	40055	860	483	59196	17588	0	17285	477	0
	Zhejiang	2268	58616	2319	3	20507	11559	0	7025	1655	1
	Shanghai	275	818	1	0	1772	2944	0	1913	727	0
	Jiangsu	3362	7787	84	942	43293	21103	0	25426	4264	0
	Shandong	3997	25383	670	2379	77242	28206	0	13254	2463	0
Central	Hubei	3047	83936	8865	898	53243	14172	0	19837	615	0
	Hunan	3425	121363	5804	18520	45150	16336	0	12585	2362	0
	Henan	3560	37362	6601	2579	79419	24495	0	14445	393	0
North	Shanxi	2420	43611	17346	31064	45105	10185	0	1731	546	0
	Hebei	3666	44371	19883	19492	70400	21094	0	5711	1428	0
	Beijing	401	5977	3701	146	2509	3176	0	618	32	0
	Inner Mongolia	21228	167115	76564	543772	115508	14975	0	10645	38094	0
	Tianjin	453	1852	0	153	3296	3319	0	2373	327	0
Northeast	Liaoning	2654	52080	8077	4886	57100	13302	0	6916	2864	0
	Jilin	272	15733	53	86	9303	1125	0	1001	82	0
	Heilongjiang	5043	214459	1773	11864	172578	11671	0	16864	35010	0
Northwest	Shaanxi	2804	106245	18515	22109	41483	9204	0	2733	487	0
	Gansu	1320	11968	4488	149072	93632	15840	0	5984	10736	0
	Xinjiang	5172	40832	81293	519885	81087	14163	22242	30842	15245	0
	Ningxia	942	9537	0	20312	11984	2973	0	1688	249	0
	Qinghai	3125	9096	36940	394727	6265	4909	4233	20233	51012	0
Southwest	Guizhou	3174	79346	32755	1888	34726	7751	0	2554	71	0
	Chongqing	1433	38067	8823	237	21508	6426	0	2717	150	0
	Xizang (Tibet)	1596	98180	80782	800653	4540	1642	20715	38589	43025	0
	Yunnan	5219	220773	28917	13238	79676	10773	431	5654	398	0
	Sichuan	4492	183471	70724	96884	64302	18496	459	10073	12309	0
Note:		TR=Traffic route; TC=Tree cover; SL=Shrubland; GL+BL&SV=the total of 'Grassland' and 'Barren and sparse vegetation'; CL=Cropland; BD=Building; S&I=Snow and ice; WT=Water; WL=Wetland; M&L=Moss and lichen.										

For the second comment, we agree that the optical images have difficulty in classifying forest swamps and other similar land-cover types. According to your suggestion, we supplemented the land-cover mapping results of the SinoLC-1 in three challenging landscapes. Figure 15 of the manuscript (Figure R1-6 of the response letter) demonstrates three special landscapes that are challenging to distinguish in VHR optical images and even HR multispectral images. The three landscapes include (a) Marshland (i.e., muddy areas with dense water and grass that have been soaked in stagnant water) captured from the Daqing Longfeng Wetland Nature Reserve, Heilongjiang Province, which is the largest urban wetland in China, (b) Forest swamp (i.e., the landscape dominated by trees or shrubs formed under humid soil, stagnant water, or shallow water layers) captured from Chongming island, Shanghai City, which is known as the world's largest estuarine alluvial island wetland, and (c) Watercourse (the route through which river water flows, usually referring to navigable waterways) captured from the Beijing-Hangzhou Grand Canal.

To show the scientific significance and applicability of SinoLC-1, we illustrated the VHR Google Earth image, the SinoLC-1, the Sentinel-2 image, and three 10-m land-cover products in these landscapes. As shown in Figure R1-6 (a), the SinoLC-1 reveals most of the marshland in the area and distinguishes the surrounding water and grasslands. Among the three 10-m land-cover products generated from the Sentinel image, the ESA_GLC10 accurately reflects the marshland in the area, but the FROM_GLC10 and ESRI_GLC10 miss the majority of wetland type. As shown in Figure R1-6 (b), it is observed that the VHR optical image shows more clear spatial detail than the 10-m Sentinel image. From the perspective of the land-cover map, the SinoLC-1 shows the forest swamp (i.e., land cover type of wetland in the legend), rivers, and tree canopy content in the area. The ESRI_GLC10 shows an accurate result on the forest swamp landscape. The ESA_GLC10 overestimates the tree canopy type, and the FROM_ GLC10 overestimates the cropland. As shown in Figure R1-6 (c), the SinoLC-1 accurately reflects the watercourse, and due to the fine spatial resolution, the bridges on the watercourse are also clearly displayed. Among the three 10-m land-cover products generated from the Sentinel image, the ESRI_GLC10 and FROM_GLC10 have acceptable classification results on the watercourse. However, the FROM_ GLC10 only shows the central part of the watercourse and underestimates the width. For ESA_GLC10, the watercourse was incorrectly classified into the land-cover type of 'barren and low vegetation'.
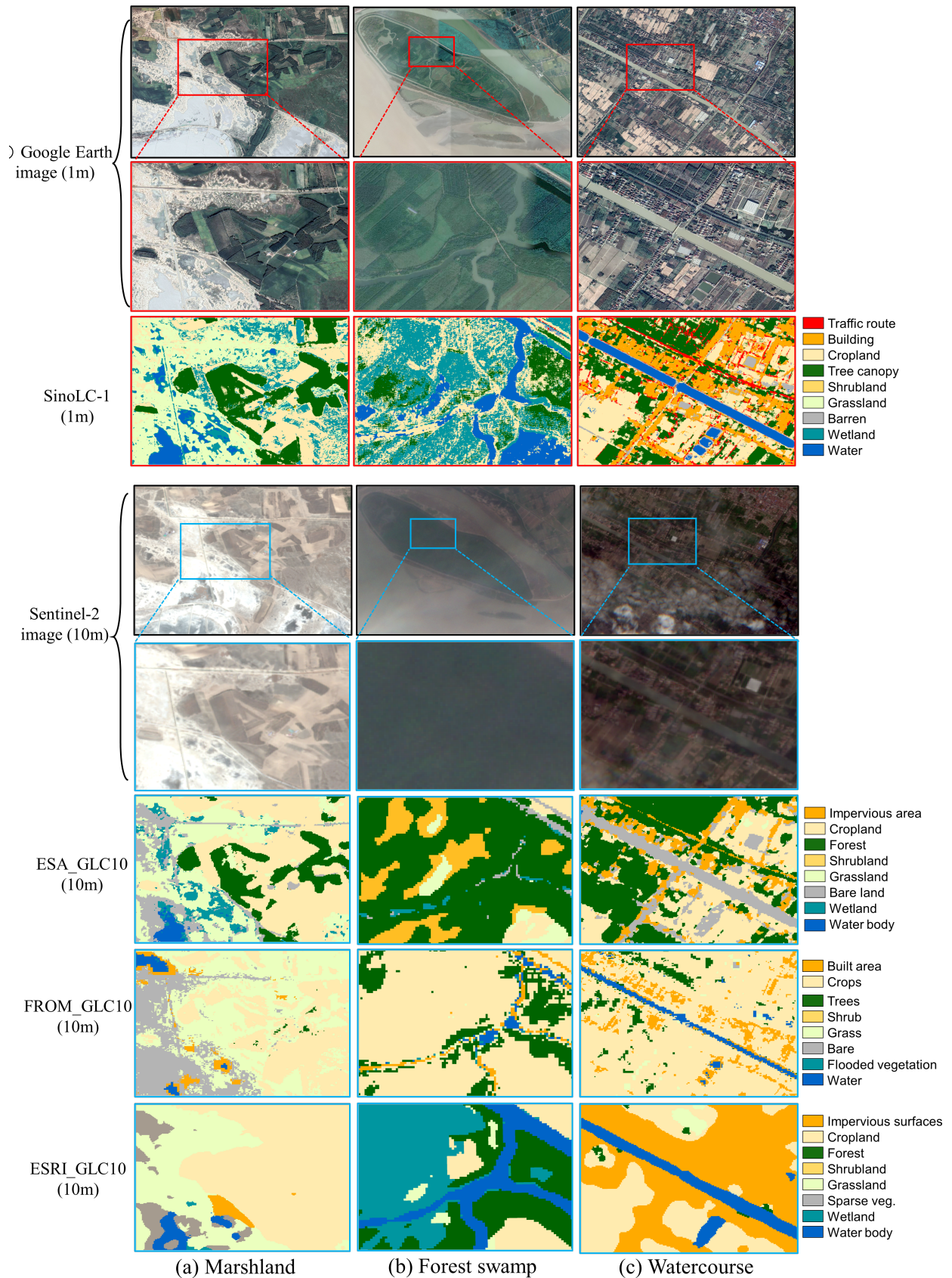
Figure R1-6. Demonstrations of the visual comparison for challenging land-cover types which include (a) Marshland, (b) Forest swamp, and (c) Watercourse. The VHR remote sensing images in the figure are from © Google Earth 2021.

(5) Add legends to all maps to address the current difficulty of comparing different product qualities, such as Figure 13.

Response:

Thanks for your constructive suggestions. We have supplemented the legends to all maps in Figures 8, 13, and 14 of the revised manuscript (Figures R1-7, R1-8, and R1-9). In the comparison of different products, we demonstrated the original land-cover types of different products and unified the color of similar land-cover types for better visual comparison.
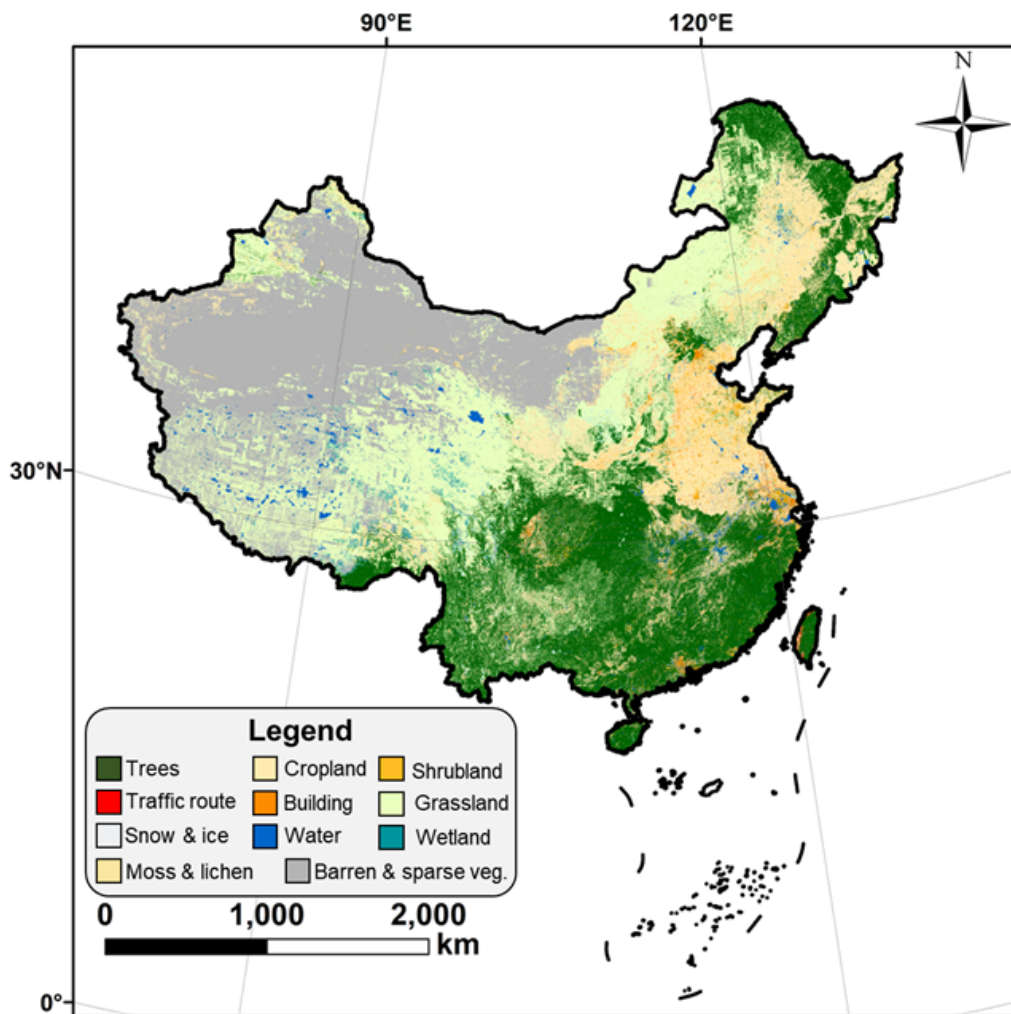
Figure R1-7. Demonstration of SinoLC-1: a 1-meter-resolution national-scale land-cover map of China.

(a) © Google Earth image (1m)
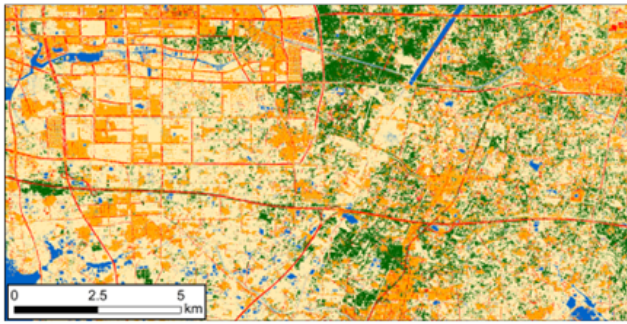
■ Traffic route	■ Building	■ Cropland	■ Tree canopy	■ Shrubland
■ Water	■ Grassland	■ Barren	■ Wetland	

(b) SinoLC-1 (1m)
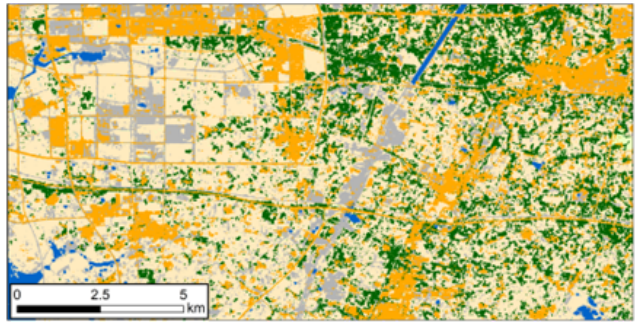
■ Built-up	■ Cropland	■ Trees	■ Shrubland
■ Open water	■ Grassland	■ Barren	■ Herbaceous wetland

(c) ESA_GLC10 (10m)

■ Impervious area	■ Cropland	■ Forest	■ Shrubland
■ Water body	■ Grassland	■ Bare land	■ Wetland

(d) FROM_GLC10 (10m)

■ Built area	■ Crops	■ Trees	■ Shrub
■ Water	■ Grass	■ Bare	■ Flooded vegetation

(e) ESRI_GLC10 (10m)

■ Impervious surfaces	■ Cropland	■ Forest	■ Shrubland
■ Water body	■ Grassland	■ Sparse veg.	■ Wetland

(f) GLC_FCS30 (30m)
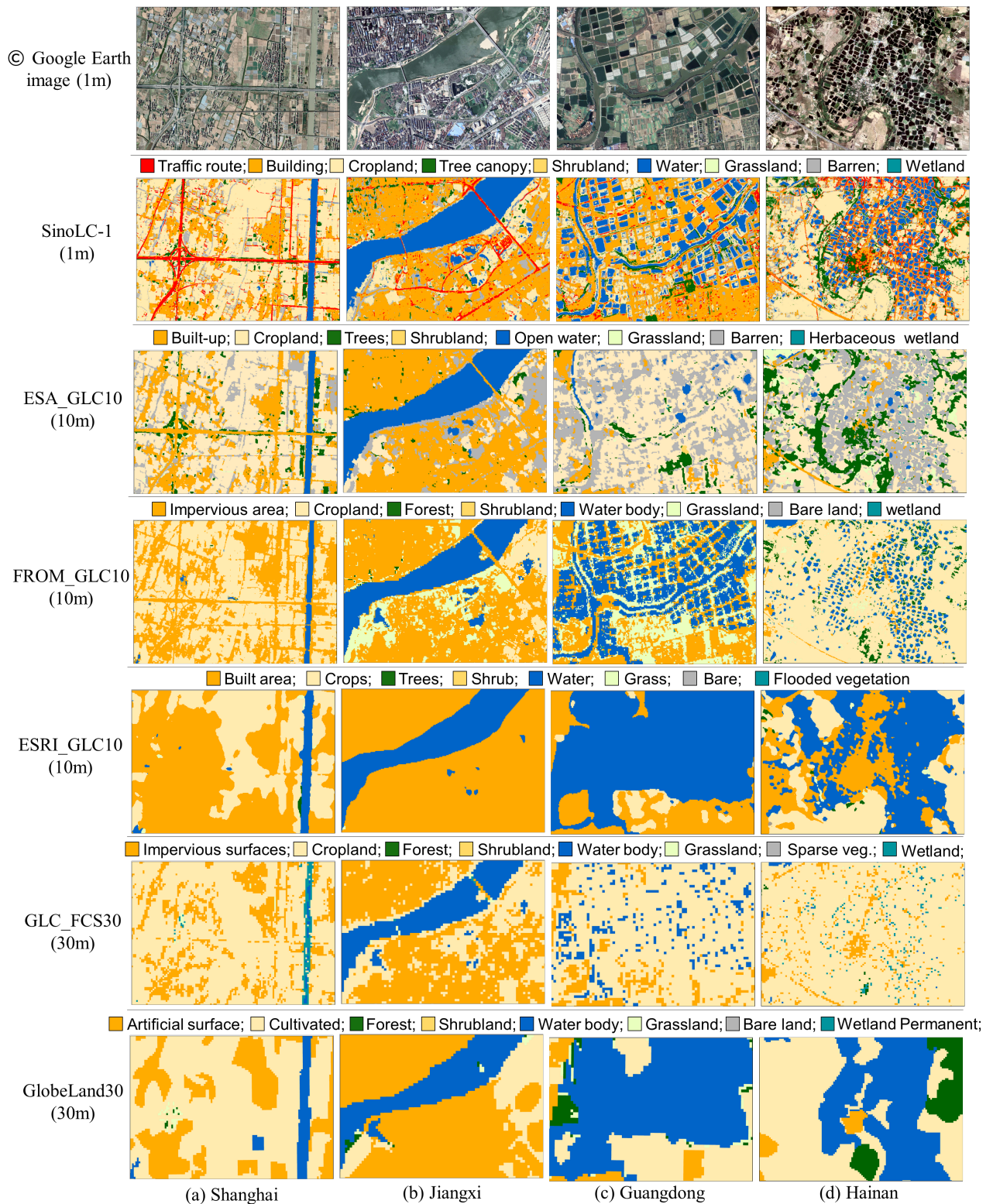
■ Artificial Surface	■ Cultivated land	■ Forest	■ Shrubland
■ Water body	■ Grassland	■ Bare land	■ Wetland permanent

(g) GlobeLand30 (30m)

Figure R1-8. Demonstration of the visual comparison for Changzhou City, Jiangsu Province. The VHR remote sensing image in the figure is from © Google Earth 2021.

© Google Earth image (1m)

Traffic route; Building; Cropland; Tree canopy; Shrubland; Water; Grassland; Barren; Wetland

SinoLC-1 (1m)

Built-up; Cropland; Trees; Shrubland; Open water; Grassland; Barren; Herbaceous wetland

ESA_GLC10 (10m)

Impervious area; Cropland; Forest; Shrubland; Water body; Grassland; Bare land; wetland

FROM_GLC10 (10m)

Built area; Crops; Trees; Shrub; Water; Grass; Bare; Flooded vegetation

ESRI_GLC10 (10m)

Impervious surfaces; Cropland; Forest; Shrubland; Water body; Grassland; Sparse veg.; Wetland;

GLC_FCS30 (30m)

Artificial surface; Cultivated; Forest; Shrubland; Water body; Grassland; Bare land; Wetland Permanent;

GlobeLand30 (30m)

(a) Shanghai   (b) Jiangxi   (c) Guangdong   (d) Hainan

Figure R1-9. Demonstrations of the visual comparison for four typical regions. The VHR remote sensing images in the figure are from © Google Earth 2021.

(6) The authors utilized current global-scale land cover products as mapping samples, but the quality of them in the Chinese region is uncertain. The quality of these products in the Chinese region is not always robust according to the text and figures in section 4.2 of the manuscript. Therefore, how do the authors account for these variables that might affect SinoLC-1's quality?

Response:

Thank you for your constructive comment. We agree that using global-scale land-cover products as training data for SinoLC-1 may bring uncertainty. To be clearer and in accordance with your concerns, we would like to respond to this question from three aspects, including (1) Analyzing the sources of uncertainty in training labels; (2) Analyzing how we reduce the uncertainty during sample selection and network training; (3) Comprehensively analyzing the impact of uncertainty on the SinoLC-1 mapping results.

- (1/3) Unstable sample brought by the low-resolution, outdated, noisy training labels.

    The manual annotation of labeled data is laborious and time-consuming, which challenges the efficiency, expenditure, and applied coverage of the VHR land-cover mapping. Based on this situation, the SinoLC-1 dataset was produced by using low-resolution land-cover products as training labels. According to the production of SinoLC-1, we sorted out the noise sources of labeled data into three main parts:

    (a) Spatial resolution mismatch

    There is a resolution gap between the 1-meter images and the 10-meter labels. The coarse label brought noisy samples to the fine edges and texture info of VHR images during the training process.

    (b) Temporal mismatch

    There is a temporal gap between the VHR images and the adopted 10-meter resolution GLC products. The land-cover maps produced at different time points brought noisy samples.

    (c) Product defects:

    Due to the defects of classifiers and the insufficient image quality, the using GLC products may have incorrect results, which brought labeling errors and noisy samples to the production of SinoLC-1.

    Figure R1-10 shows the samples of these three main noise sources and the results of the SinoLC-

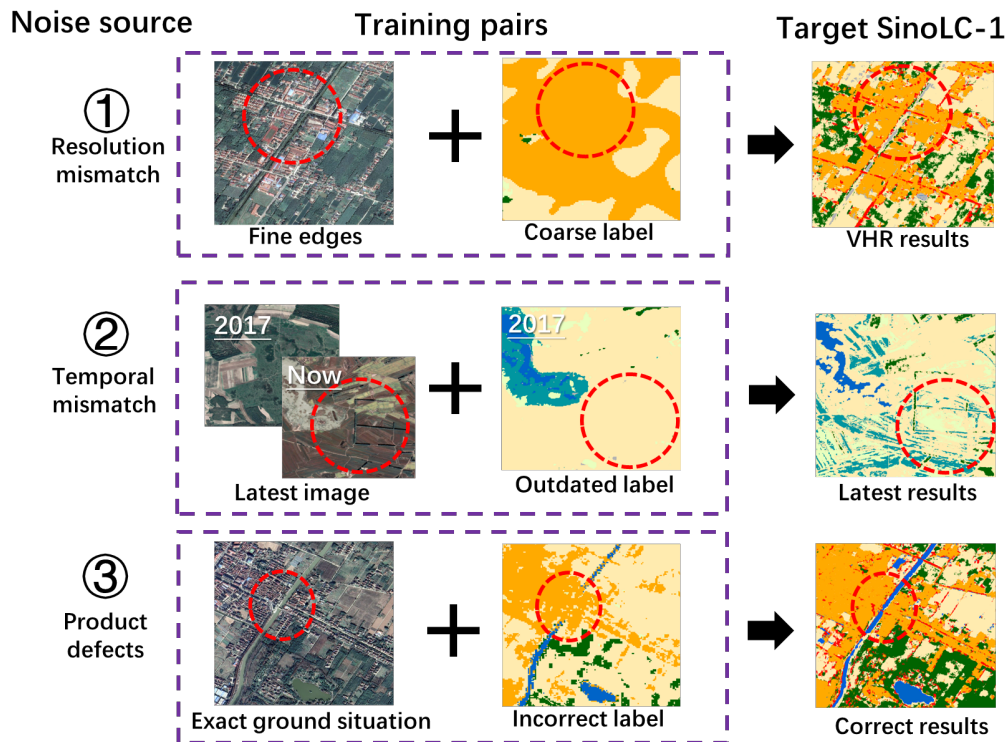1 which are accurate and consistent with the VHR images.

Figure R1-10. Demonstration of the main uncertainty and unstable samples exiting in the training labels

- (2/3) Reliable training sample collection and network training process.

To reduce the impact of uncertainty during the production of SinoLC-1, we conducted a reliable sample collection and network training process. Firstly, Figure R1-11 shows the details of the training sample collection process. The land-cover types of three 10-m global land-cover products were unified, and then they were intersected to generate the label-selected mask. In the selected mask, the pixels/areas, where their land-cover types were the same in the three GLC products, would be preserved as the stable labeled areas; otherwise, the pixels/areas would be set as unlabeled type and maintained void value. As an example of the selected training sample shown in Figure R1-12, we demonstrate three typical areas where the first area shows a preserved correct sample (three GLC products have the same type), the second area shows an inaccurate sample (partial samples are abandoned), and the third area shows an incorrect sample (the samples are completely abandoned). Based on this sample collection process, the stable parts of these GLC products were preserved and the uncertain parts were abandoned, which ensures the reliability of the training labels. Secondly, to address the noisy label issue, the low-to-high network (L2HNet) was designed with a weakly-supervised based Confident Area Selection

(CAS) module and a self-supervised loss function. As the network training process shown in Figure R1-13, the CAS module selects the high-confident samples from the coarse, outdated, and noisy labels based on the confidence probability of the prediction batches. For the loss calculation, the Cross-Entropy (CE) loss is only calculated on the selected confident area, and the vague area (with low confidence probability) is ignored in the CE loss calculation. Then, the self-supervised Dynamic Vague Area (DVA) loss is calculated between the confident area and the vague area by constraining the feature similarity of the same land-cover types. Based on these components, the L2HNet enables to learn reliable information from the coarse, outdated, noisy labels, and the capacity of L2HNet to utilize noisy labels for accurate large-scale VHR land mapping has been validated in numerous datasets (Li et al., 2022).

In general, by combining the reliable training sample collection and network training process, the impact of uncertainty in training labels could be reduced to a certain extent during the production of SinoLC-1.
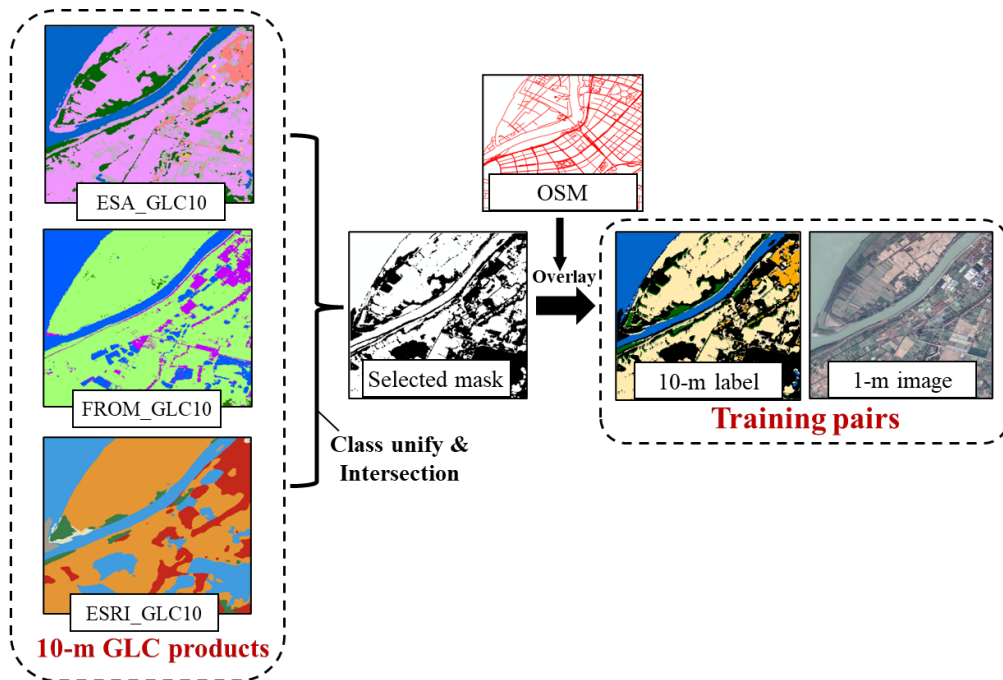
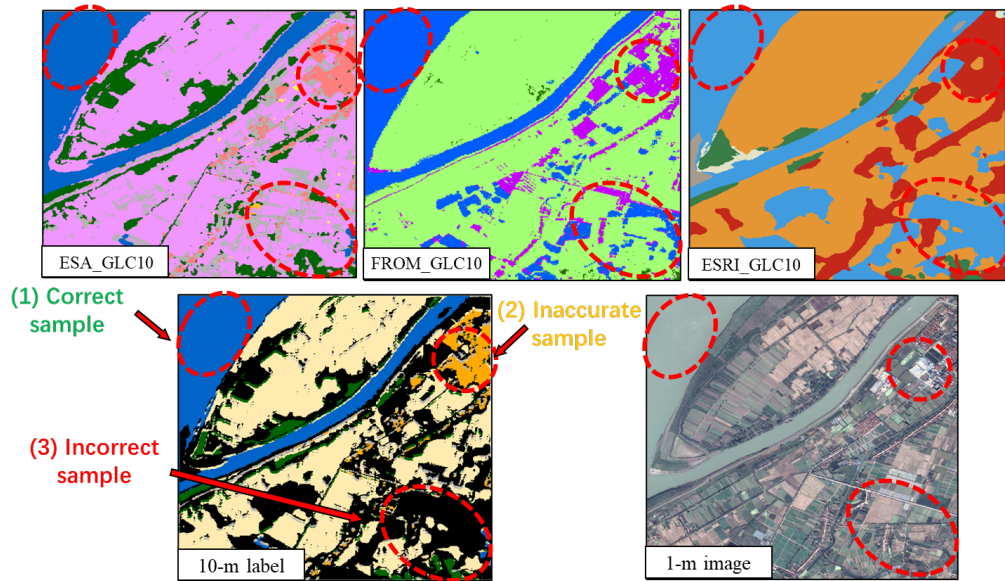**Figure R1-11. Demonstration of the training sample collection process**

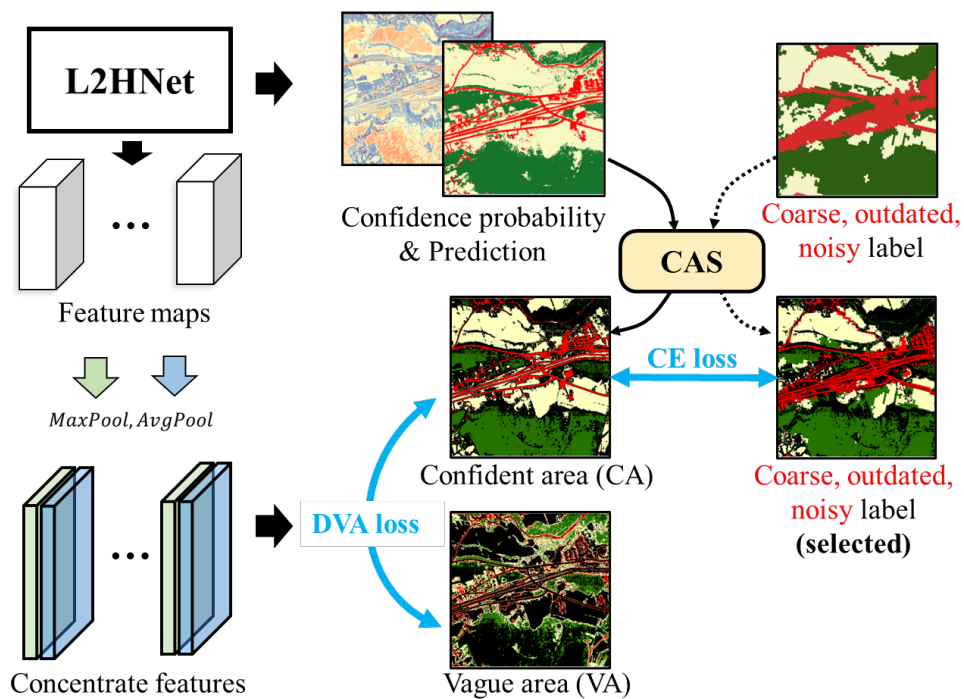**Figure R1-12. Demonstration of the selected training samples**

Figure R1-13. Demonstration of the training process of the land-cover mapping network.

- (3/3) Comprehensively analyzing the impact of uncertainty on mapping results.

    To comprehensively analyze the uncertainty of three global land-cover products, which were used to generate the SinoLC-1, more rigorously, we added two widely used open-access validation datasets to assess the accuracy of five global-scale products (including three utilized 10-m products and other two 30-m products) across China. Figure R1-14 shows the

supplemented workflow added to comprehensively evaluate the accuracy and uncertainty of the SinoLC-1 and other land-cover products. We have fully evaluated their producer accuracy (P.A.), user accuracy (U.A.), overall accuracy (O.A.), and kappa coefficients for each land-cover type in China, which are presented in Table R1-8, Figure R1-19, and Figure R1-20. We also analyzed their potential impact on the production process of SinoLC-1 comprehensively.
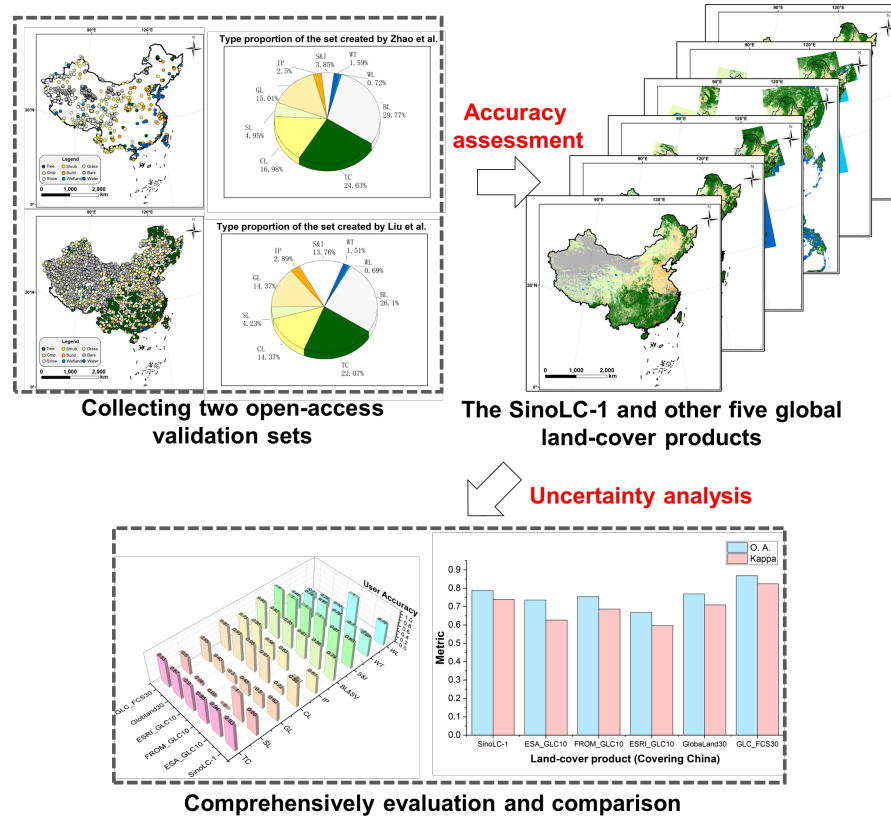
Figure R1-14. The supplemented workflow to evaluate the accuracy and uncertainty of the SinoLC-1 and other five global land-cover products

Firstly, the utilized two open-access validation datasets are created based on multiple data sources and manual verification, reporting a stable quality and high independence. The detailed information on these validation sets is as follows:

(a) Validation set created by Liu et al. DOI: https://doi.org/10.5281/zenodo.3551995

Liu et al. (2019) created a global land-cover validation set by combining several existing reference datasets such as the GLCNMO2008 training dataset, VIIRS reference dataset, STEP reference dataset, Global cropland reference data, and so on to guarantee the confidence and objective of the validation samples. Furthermore, high-resolution imagery in Google Earth and time-series NDVI, NDSI values of each related point were integrated to derive the validation datasets.
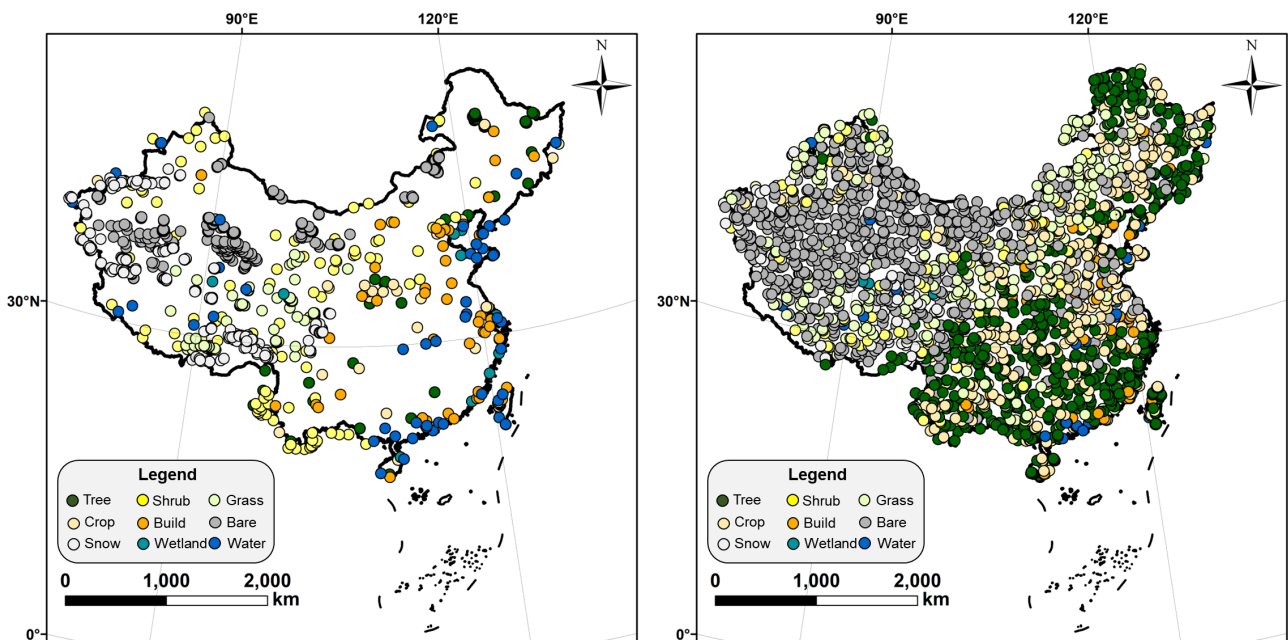
(b) Validation set created by Zhao et al. DOI:

Zhao et al. (2014) created a global land-cover validation set with a total of 38,664 sample units by interpreting Landsat images and MODIS EVI time series data, as well as high-resolution images from Google Earth, recording the quality of reference data, and interpreter confidence. Zhao et al. confirmed that the dataset had been carefully improved through several rounds of interpretation and verification by different image interpreters, and checked by one quality controller. Independent test interpretation indicated that the quality control correctness level reached 90% at level 1 land-cove type.

According to the description of the data providers, these validation sets contain two levels of land-cover types, and their spatial distribution and classification system are shown in Figure R1-15, Table R1-7, and Table R1-8.

The cited references of this response are as follows:

Zhao, Y., Gong, P., Yu, L., Hu, L., Li, X., Li, C., Zhang, H., Zheng, Y., Wang, J., Zhao, Y. and Cheng, Q. (2014). Towards a common validation sample set for global land-cover mapping. International Journal of Remote Sensing, 35(13), 4795-4814. https://doi.org/10.1080/01431161.2014.930202

Liu, L., Gao, Y., Zhang, X., Chen, X., & Xie, S. (2019). A Dataset of Global Land Cover Validation Samples (Version v1) [Data set]. Zenodo. https://doi.org/10.5281/zenodo.3551995

(a) Validation set created by Liu et al.   (b) Validation set created by Zhao et al.

Figure R1-15. Demonstration of two open-access validation set.

Table R1-4. The classification system of the validation set created by Liu et al.

Level 1 type	Level 2 type	Sample count	Total	Proportion (%)
Cropland	Rainfed cropland	44	353	14.33%
	Herbaceous cover	0		
	Irrigated cropland	311		
Forest	Evergreen broadleaved forest	123	542	22.01%
	Deciduous broadleaved forest	303		
	Mixed leaf forest	116		
Shrubland	Shrubland	78	104	4.22%
	Evergreen shrubland	26		
Grassland	Grassland	360	360	14.62%
Wetlands	Wetlands	17	17	0.69%
Impervious surfaces	Impervious surfaces	71	71	2.88%
Bare areas	Sparse vegetation	285	641	26.03%
	Bare areas	329		
	Consolidated bare areas	3		
	Unconsolidated bare areas	24		
Water body	Water body	37	37	1.50%
Permanent ice and snow	Permanent ice and snow	338	338	13.72%

Table R1-5. The classification system of the validation set created by Zhao et al.

Level 1 type	Level 2 type	Sample count	Total	Proportion (%)
Crop	Rice	3	353	16.98%
	Greenhouse	1		
	Other	349		
Forest	Broadleaf	303	512	24.63%
	Needleleaf	81		
	Mixed	114		
	Orchard	14		
Grass	Managed	0	312	15.01%
	Nature	312		
Shrub	Shrub	103	103	4.95%
Wetland	Grass	15	15	0.72%
	Silt	0		
Water	Lake	7	33	1.59%
	Pond	19		
	River	7		
	Sea	0		
Impervious	High albedo	19	52	2.50%
	Low albedo	33		
Bare land	Saline-Alkali	10	619	29.77%
	Sand	138		
	Gravel	303		
	Bare-cropland	89		
	Dry river/lake bed	2		
	other	77		
Snow and Ice	Snow	80	80	3.85%
	Ice	0		

Secondly, to comprehensively validate the accuracy and uncertainty of the SinoLC-1, we calculated the confusion matrix of SinoLC-1 and further validated its P.A., U.A., O.A., and kappa coefficient based on two open-access validation sets. As shown in Table R1-6 and Table R1-7, the

O.A. of the SinoLC-1 validated on the validation sets created by Liu et al. and Zhao et al. are 78.80% and 64.69%, respectively. The Kappa of the SinoLC-1 validated on the validation sets created by Liu et al. and Zhao et al. are 0.7394 and 0.5588, respectively. Furthermore, to illustrate more detailed assessment results, Figure R1-16 shows the corresponding confusion proportions for each considered land-cover type of the SinoLC-1 validated on two datasets.

Table R1-6. Confusion matrix for the SinoLC-1 according to the validation set created by Liu et al.

Classification	TC	SL	GL	CL	IP	BL&SV	S&I	WT	WL	Total	P.A. (%)
Tree Cover	421	5	80	32	0	2	1	1	0	542	77.68
Shrubland	7	34	32	2	0	27	2	0	0	104	32.69
Grassland	2	2	342	0	0	7	0	0	0	353	96.88
Cropland	5	1	3	316	29	3	0	3	0	360	87.78
Impervious	7	0	3	7	51	3	0	0	0	71	71.83
Barren &Sparse veg.	1	7	12	0	0	616	5	0	0	641	96.10
Snow and ice	1	0	78	0	0	121	136	2	0	338	40.24
Water	7	0	0	5	3	1	0	19	2	37	51.35
Wetland	0	0	1	4	0	1	2	3	6	17	35.29
Total	451	49	551	366	83	781	146	28	8	2463	
U.A. (%)	93.35	69.39	62.07	86.34	61.45	78.87	93.15	67.86	75.00		
O.A. (%)					78.80						
Kappa					0.7394						

Note: TC=Tree cover; SL=Shrubland; GL=Grassland; CL=Cropland; IP=Impervious (Building and traffic route); BL&SV=Barren and sparse vegetation; S&I=Snow and ice; WT=Water; WL=Wetland

Table R1-7. Confusion matrix for the SinoLC-1 according to the validation set created by Zhao et al.

Classification	TC	SL	GL	CL	IP	BL&SV	S&I	WT	WL	Total	P.A. (%)
Tree Cover	376	13	60	35	6	7	1	5	9	512	73.44
Shrubland	10	34	33	3	0	21	2	0	0	103	33.01
Grassland	37	2	215	20	3	33	0	1	1	312	68.91
Cropland	83	1	36	191	18	21	0	2	1	353	54.11
Impervious	3	0	4	13	29	3	0	0	0	52	55.77
Barren &Sparse veg.	13	7	109	62	6	411	5	5	1	619	66.40
Snow and ice	1	0	5	0	0	8	65	1	0	80	81.25
Water	6	0	0	7	2	2	0	16	0	33	48.48
Wetland	0	0	2	0	1	2	2	0	8	15	53.33
Total	529	57	464	331	65	508	75	30	20	2079	
U.A. (%)	71.08	59.65	46.34	57.70	44.62	80.91	86.67	53.33	40.00		
O.A. (%)					64.69						
Kappa					0.5588						

Note: TC=Tree cover; SL=Shrubland; GL=Grassland; CL=Cropland; IP=Impervious (Building and traffic route); BL&SV=Barren and sparse vegetation; S&I=Snow and ice; WT=Water; WL=Wetland
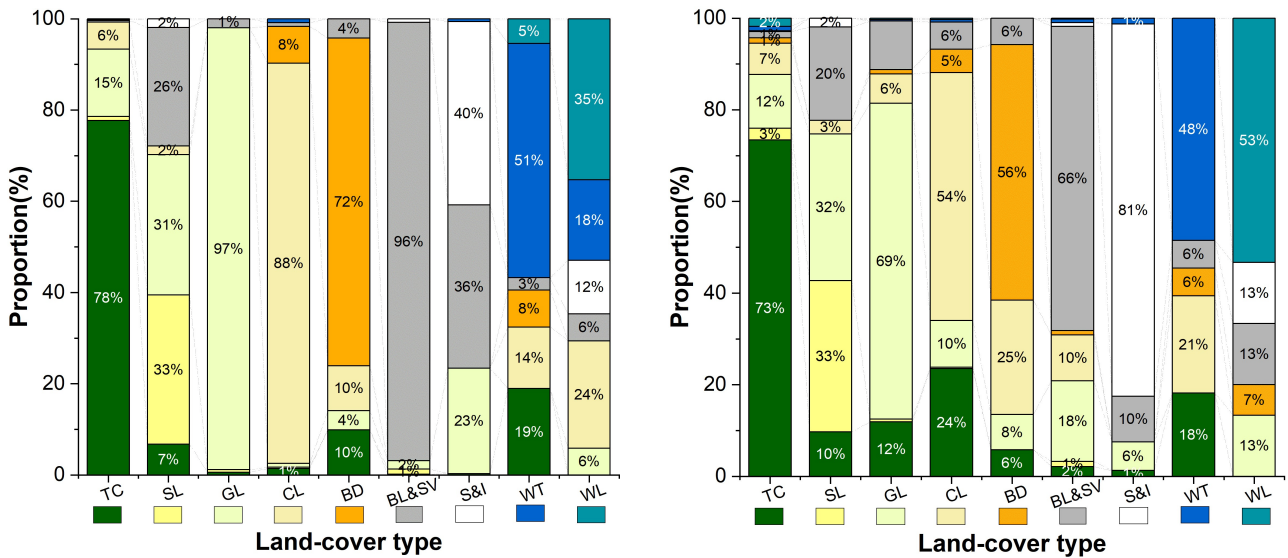
(a) Confusion proportions for land-cover type of the SinoLC-1 validated with the set created by Liu et al.

(b) Confusion proportions for land-cover type of the SinoLC-1 validated with the set created by Zhao et al.

**Figure R1-16. Confusion proportions of the validation results.**

Thirdly, to assess the uncertainty impact of three utilized 10-m land-cover products more rigorously and transparently, and to conduct a more complete comparison, we used these validation sets to validate the accuracy of five comparative land-cover datasets (including three utilized 10-m products and other two 30-m products). Figure R1-17 and Figure R1-18 show the spatial distribution of two validation sets among five comparative land-cover products in China. For clearer expression, we mark the validation set created by Liu et al. (2019) as S1 and mark the set created by Zhao et al. (2017) as S2.

The comparison results are shown in Table R1-8 and Figure R1-19. From the quantitative comparison, the SinoLC-1 has the second highest O.A. on two validation sets where the SinoLC-1 has a O.A. of 0.6469 with S1 (lower than the 10-meter ESA_GLC10) and has an O.A. of 0.7881 with S2 (lower than the 30-meter GLC_FCS30). Furthermore, we compared the U.A. of every considered type between the SionLC-1 and the other five products in Figure R1-20. From the results shown in Figure R1-20 (a), the SinoLC-1 has the second highest U.A. in types of 'Tree canopy', 'Shrubland', 'Grassland', and 'Wetland' compared to the other five products, and has the U.A. of 'Cropland' and 'Impervious surface' surpassing the average of other five products. From the results shown in Figure R1-20 (b), the SinoLC-1 has the highest U.A. in types of 'Shrubland' and 'Grassland', and has the U.A. of 'Snow and ice' and 'Wetland' surpassing the average of the other five products.

In general, by quantitatively comparing the SinoLC-1 product with five widely used land-cover products on two open-access validation datasets, the produced SinoLC-1 shows acceptable confusion proportion among land-cover types and has competitive accuracy among the other land-cover products across China. The quantitative results are used to explain the uncertainty of the three training data and further demonstrate that the production process of the SinoLC-1 reduced the impact of noise labels to a certain extent. The supplemented quantitative comparison and analysis were added in Section 4.2.2 of the revised manuscript.
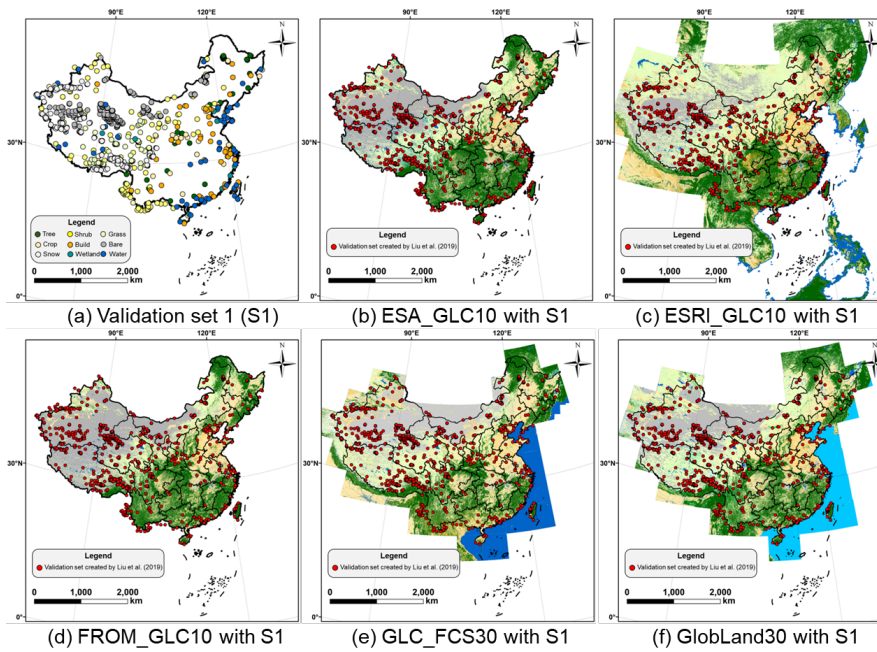
Figure R1-17. Demonstration of five comparison products and the validation set (S1) created by Liu et al.
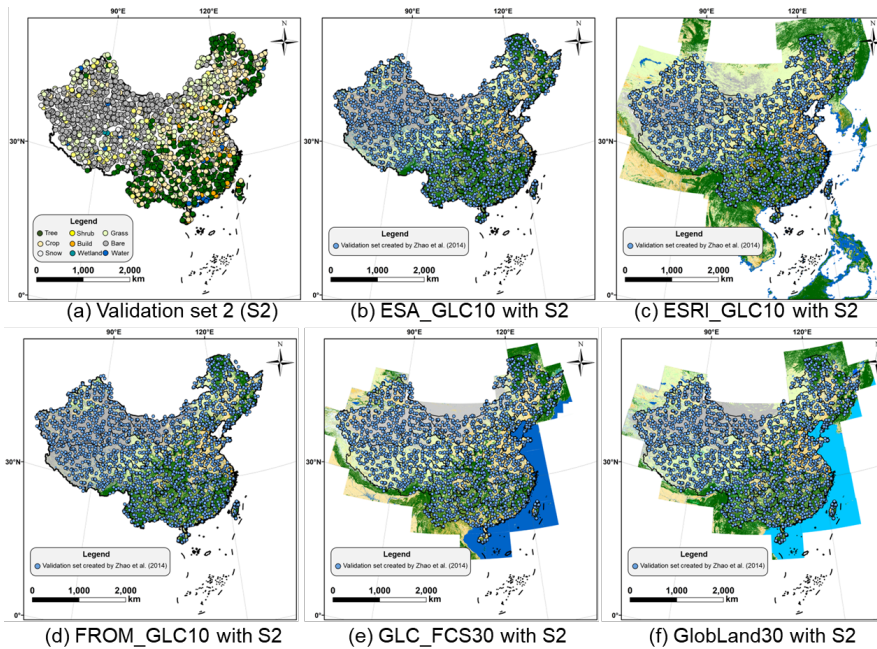
Figure R1-18. Demonstration of five comparison products and the validation set (S2) created by Zhao et al.

**Table R1-8. Quantitative comparison between the SionLC-1 and other five land-cover products.**

Metric Dataset	Validation set of Zhao et al.		Validation set of Liu et al.	
	O. A.	Kappa	O. A.	Kappa
SinoLC-1	0.6469	0.5588	0.7881	0.7394
ESA_GLC10	0.6646	0.5722	0.7356	0.6269
FROM_GLC10	0.6411	0.5942	0.7538	0.6871
ESRI_GLC10	0.6232	0.5210	0.6675	0.5972
GlobaLand30	0.6209	0.5285	0.7694	0.7090
GLC_FCS30	0.5778	0.4675	0.8684	0.8241
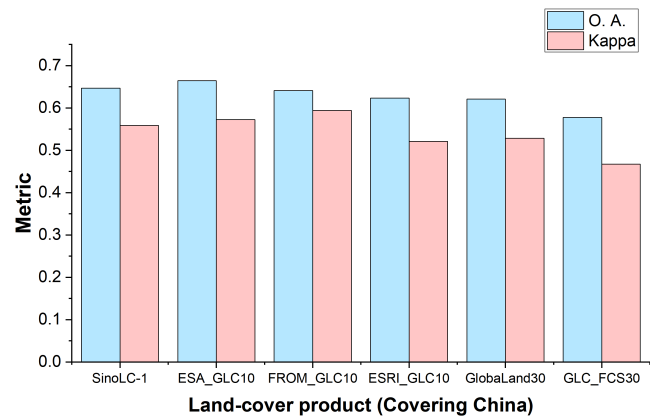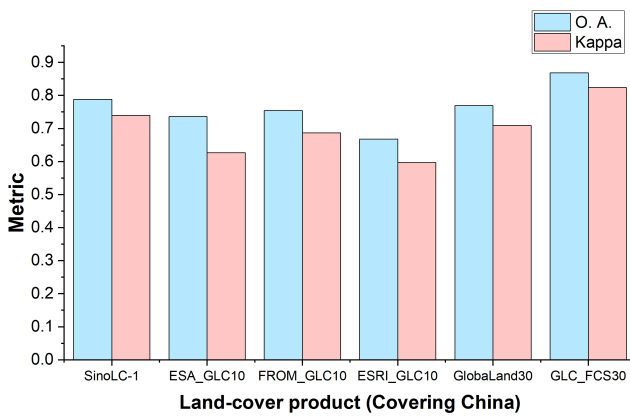
(a)   The validation results based on S1

(b)   The validation results based on S2

Figure R1-19. The quantitative validation and comparison of the SinoLC-1 and other five products
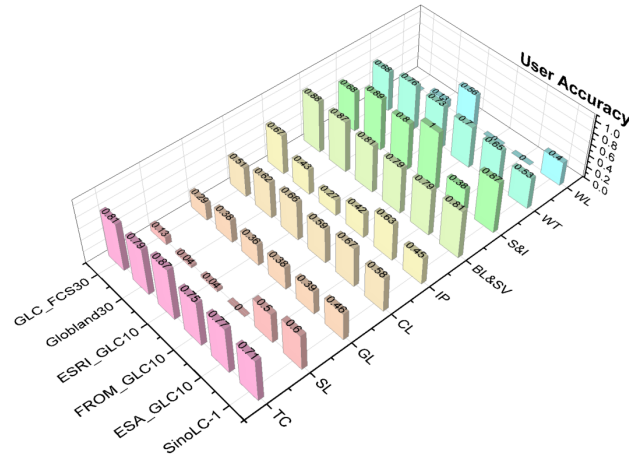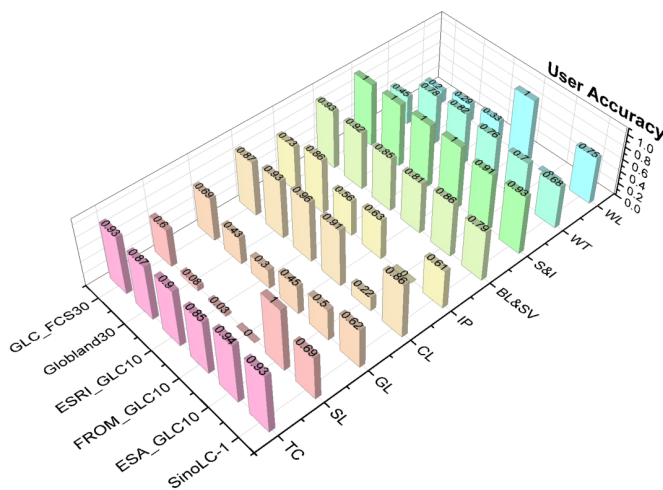
(a)   The U.A. comparison based on S1

(b)   The U.A. compassion based on S2

Figure R1-20. The U.A. comparison of the SinoLC-1 and other five products

(7) It is challenging to automatically map forests, shrubs, grasslands, wetlands, and tundra using medium-resolution images. To help the reader comprehend the characteristics of various land cover types in Google images, it is advised that the authors change Figure 6 by adding VHR samples.

Response:

    Thanks for the constructive comment. We agree that some of the land-cover types are challenging to identify in medium-resolution images due to their low spatial details in the images. According to your suggestion, we have added the VHR samples captured from the 1.07-m Google Earth images for all the land-cover types of the SinoLC-1. As shown in Figure 6 of the revised manuscript (Figure R1-21 of the response letter), every land-cover type includes three VHR samples to help the readers comprehend their characteristics.
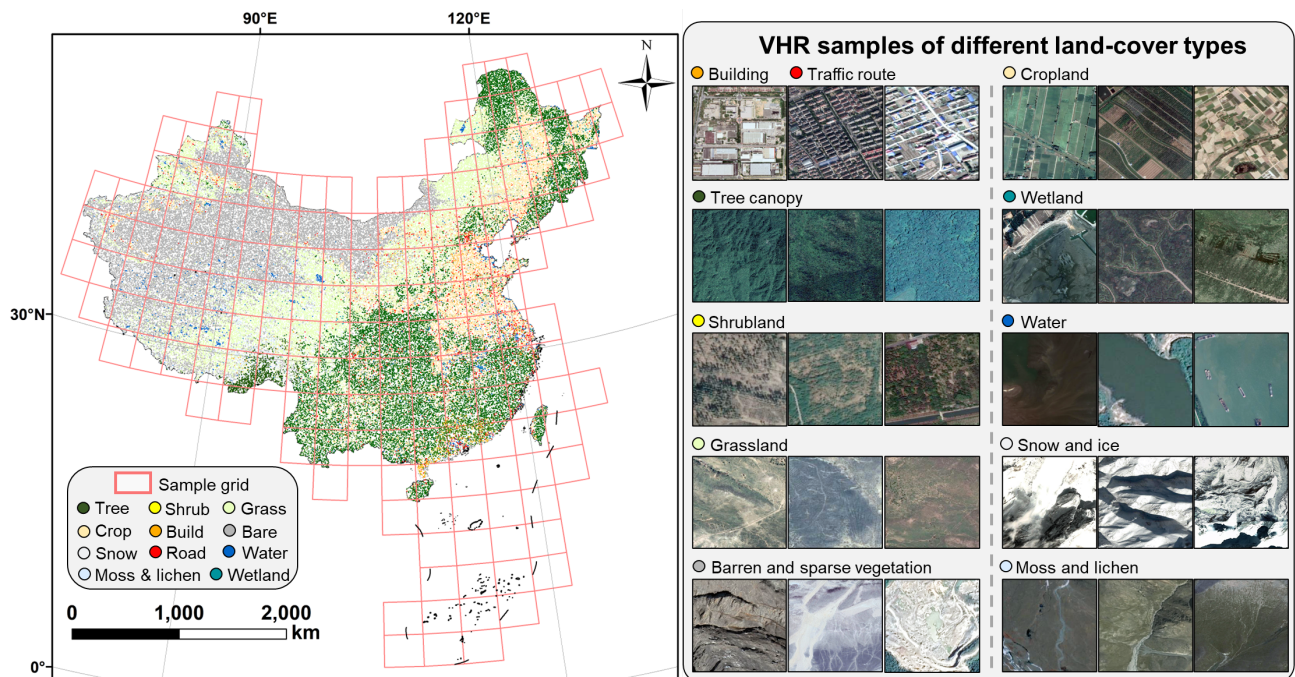
Figure R1-21. Demonstration of the sample grid, VHR samples, and the national validation sample set. Left: the spatial distributions of the sample set (the legend is written in shorter forms). Right: the VHR samples of different land-cover types collected from 1.07-m resolution © Google Earth imagery all around China.

(8) The area discrepancies between the provincial land cover categories of SinoLC-1 and NLRS are compared in Figure 17. It is important to note that the value interval on the vertical axis is too big. For instance, in Henan province, each pitch of the vertical axis corresponds to a 5,000 km² gap. Thus, the area difference between the two results cannot be well reflected for land cover categories with small areas. It is suggested that the authors seek alternative comparison methods to make the area difference between all types of land cover clear.

Response:

We appreciate this helpful feedback to increase the statistical comparison between the SinoLC-1 and 3rd NLRS. According to your feedback, we changed Figure 21 in the revised manuscript to directly illustrate the misestimation area between sinoLC-1 and 3rd NLRS under each land-cover type. To better demonstrate the differences between SinoLC-1 and 3rd NLRS, the overestimation (positive value) and underestimation (negative value) of SinoLC-1 are also reflected in Figure 21 of the manuscript (Figure R1-22 of the response letter). To make the area difference between all land-cover types clearly visible, we used breakpoints to illustrate the excessively large values of misestimation area to ensure that the land-cover types with large gaps can be reasonably displayed in the same vertical axis.

Furthermore, we have also taken your consideration in the comparison at the national scale. In the box chart shown in Figure 23 (a) of the manuscript (Figure R1-23 (a) of the response letter), we have changed the vertical axis from 'misestimation area (km²)' into 'misestimation rate', because the coverage and misestimation area of different land-cover types has significant differences, which makes it difficult to reflect in the box chart with the vertical axis of 'area (km²)'. Moreover, we supplemented Figure 23 (c) in the revised manuscript (Figure R1-23 (b) of the response letter) to show the overall misestimation rates of SinLC-1 in the whole China and evaluated the performance of Sinolc-1 from a statistical perspective which has a misestimation rate under 10% among all the land-cover types.

In addition, to demonstrate the spatial distribution of the misestimation rate for each land-cover type across China, and to provide more comparable information on the statistical assessment, we have collected the results and added the map of the misestimation rate for every land-cover type in Figure 22 of the revised manuscript (shown in Figure R1-24 of the response letter).
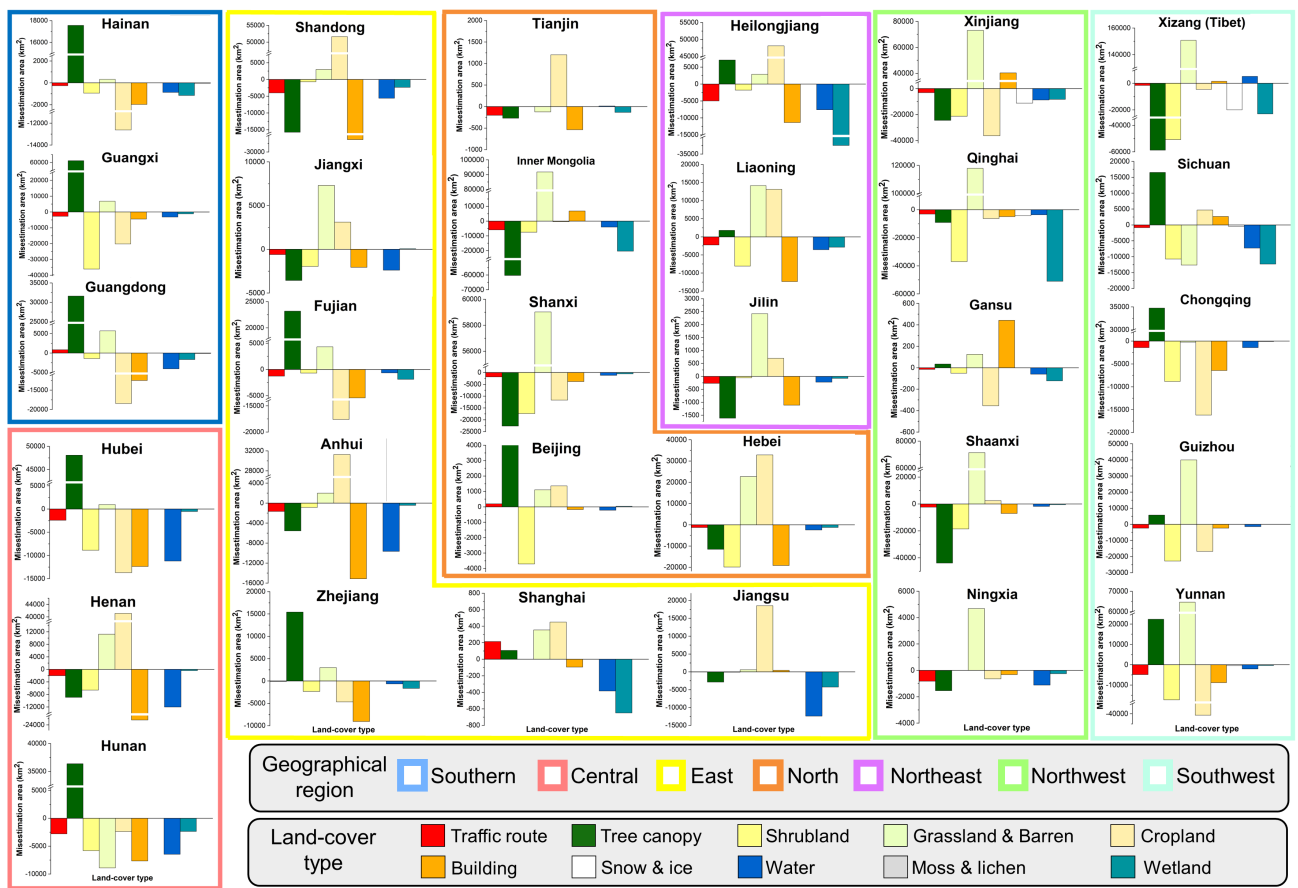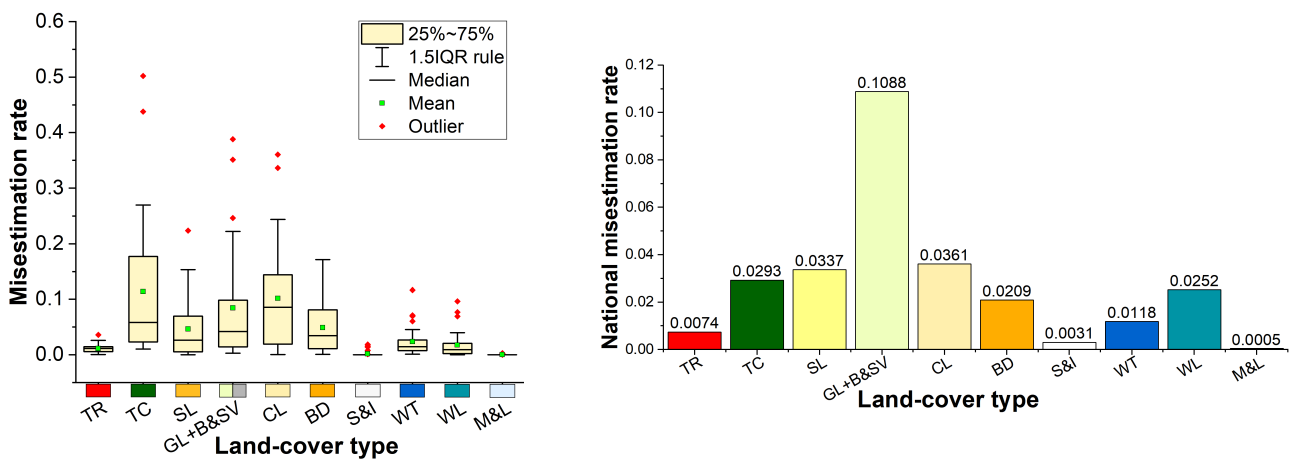
Figure R1-22. Statistical comparison between SinoLC-1 and 3rd NLRS data for 31 provinces in China. The provinces in different geographical region are represented by dissimilar wireframe colors. In every subplot, the abscissa axis represents the land-cover types, and the vertical axis represents the misestimation area.
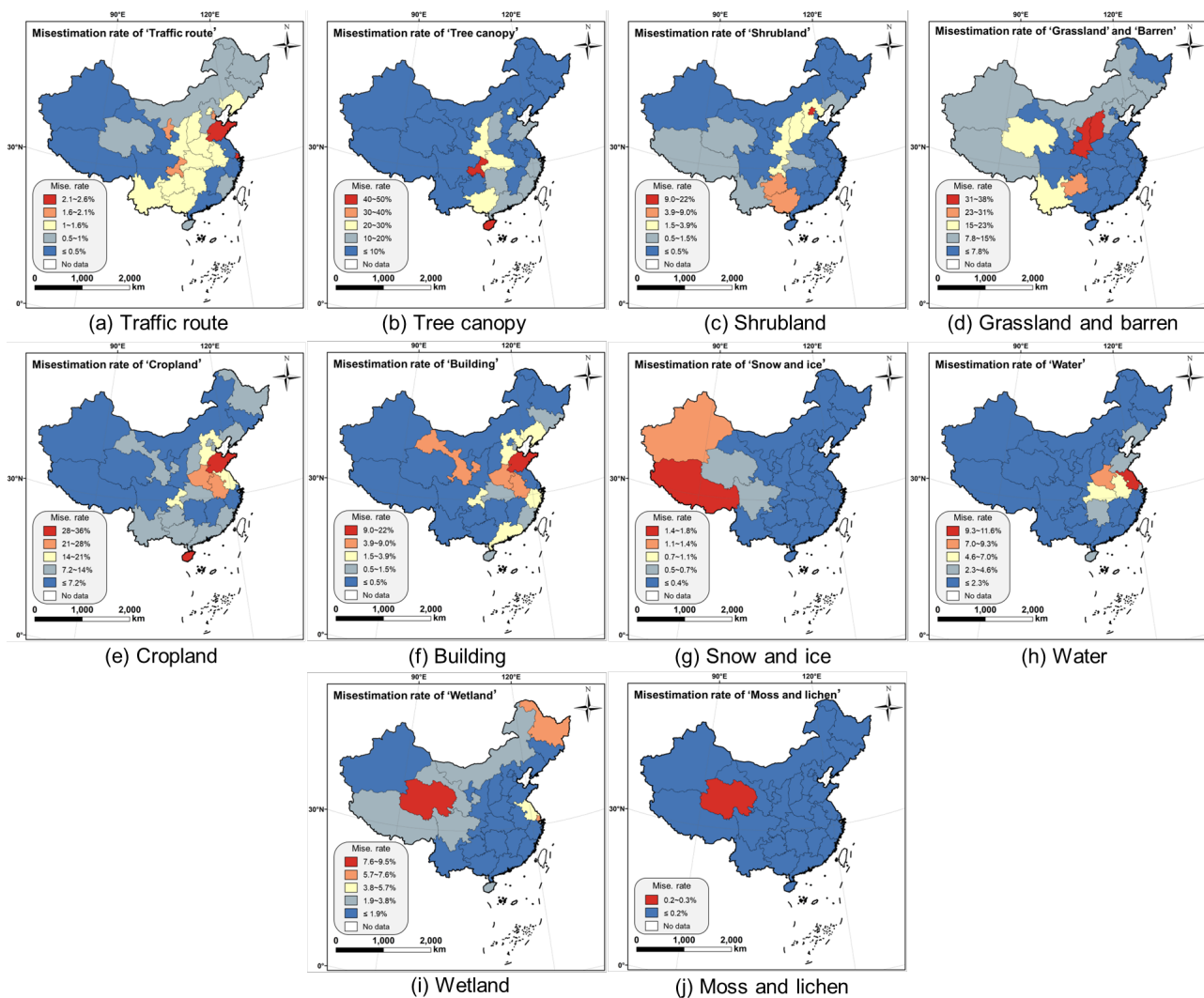

(a) Overall misestimation rate of every land-cover type through 31 provinces in China

(b) National misestimation rate of every land-cover type across China

Figure R1-23. Overall misestimation distributions in every land-cover type across China.

Figure R1-24. The misestimation rate of SinoLC-1 for 31 provinces in China. In every subplot, the statistical comparison between SinoLC-1 and 3rd NLRS data in every land-cover type is illustrated.

(9) It is advised that the authors use more inclusive language, primarily in section 4.2, where words like "worst" need to be changed.

Response:

Thank you for the comments, we have carefully checked the whole manuscript. Primarily, in Section 4.2.1, we changed the word "the worst performance" to "limited performance". Then we inclusively analyzed the performance of different products, especially comprehensive descriptions of every comparative product in different land-cover types and demonstration areas. Furthermore, the revised manuscript has been carefully proofread by a language editor, and we have made numerous changes on the expressions to make sure the language is inclusive.

(10) Checking the terms and some phrases is advised, e.g., "OBAI" in line 104 and "cropped" in line 199.

Response:

Thank you for the corrections. We have corrected the grammar issue and checked the whole manuscript with the help of language editors. We corrected the "OBAI" in line 104 to "OBIA" and changed the expression of 'cropped ' to 'divided'.